Empirical and semi-analytical methods for evaluating tunnelling-induced ground movements in sands

Andrea Franza[a], Alec M. Marshall[b],[*]

[a] *ETSI Caminos, Universidad Politécnica de Madrid, C/ Professor Aranguren s/n, 28040 Madrid, Spain*
[b] *Faculty of Engineering, University of Nottingham, University Park, NG7 2RD Nottingham, United Kingdom*

ABSTRACT

Empirical formulas and closed-form solutions provide, in many cases, good predictions of tunnelling-induced ground movements which, when combined with their computational efficiency, make them valuable for tunnel-structure interaction analyses. For sandy soils, however, there is a shortage of available methods that can adequately describe the changes in soil deformation patterns that occur as a result of tunnel volume loss, soil relative density, and geometrical parameters. In this paper, two approaches are adopted to describe centrifuge test outcomes for tunnelling in dry silica sand of varying relative density. Firstly, empirical expressions for the prediction of settlement trough shape and magnitude are presented; additionally, a set of equations is given to describe the settlement troughs using modified Gaussian curves. Next, semi-analytical expressions (modifying an elastic analytical solution for incompressible soil and ovalized tunnel) are developed to predict both vertical and horizontal movements within the ground. Results from both methods can capture the main effects that cover-to-diameter ratio, relative density, and volume loss have on surface and subsurface ground movement profiles. The proposed expressions can be used for the calibration/verification of tunnel-structure interaction analysis methods by using outputs from comparable centrifuge tests; once verified, these methods may be more widely applied to other scenarios and used within design or risk-assessment exercises.

1. Introduction

During tunnelling, stress relief and over-excavation result in movements within the soil that may cause deformations of subsurface structures and foundations. To estimate possible structural damage, greenfield tunnelling-induced ground movements need to be predicted and used within tunnel-structure interaction analyses, where the term greenfield indicates a tunnelling scenario characterised by the absence of surface or buried structures.

To simplify the problem, engineers generally focus on the steady-state ground movements occurring transverse to the tunnel axis at a distance of several tunnel diameters behind the tunnel face. Ground movements induced by the construction of bored tunnels in clay have been widely monitored and discussed (Grant and Taylor, 2000; Mair and Taylor, 1997), and their predictions using simple empirical methods are well-established (Mair et al., 1993; Peck, 1969). The mechanisms governing tunnelling-induced ground displacements in sands, however, differ from those in clays, mainly because of the lack of constraint on soil volume during shear (Marshall et al., 2012). There are a few reported case studies of tunnel construction in sands and coarse-

grained soils (Bilotta and Russo, 2012; Fargnoli et al., 2013; Hsiung, 2011; Sagaseta et al., 1999; Jaarsveld et al., 1999), and centrifuge testing has been used to study the excavation of tunnels in dense sands (Marshall et al., 2012; Vorster et al., 2005; Franza et al., in press). Recently, Franza et al. (in press) presented a parametric study using centrifuge test data to better understand the effects of soil relative density and tunnel relative depth on greenfield ground deformations in sands. This paper aims to integrate the available centrifuge test data related to greenfield ground movements in sands into computationally efficient methods (empirical expressions and semi-analytical solutions) to enable an accurate replication of the ground movements measured within the centrifuge tests.

Empirical and semi-analytical solutions can provide an efficient and reliable way of evaluating tunnelling related ground displacements and their characteristics. However, methods for tunnels in sands are only partially available; for example there is no satisfactory empirical framework for the prediction of horizontal movements in sands (Marshall, 2009; Farrell, 2010) and available empirical methods for settlement trough estimation do not incorporate the effect of soil relative density (Marshall et al., 2012). Semi-analytical solutions have been

---

Notation

a	parameter of the modified Gaussian curve
c_i	parameter of ξ
$c_{i,x/z}$	parameter of $\xi_{x/z}$
g	gravity
i	distance between the centreline and the greenfield inflection point
$\partial i/\partial z$	change in i with respect to depth (slope)
m_i	coefficient of $V_{l,t}$ in c_i
$m_{i,x/z}$	coefficient of $V_{l,t}$ in $c_{i,x/z}$
n	shape factor used in modified Gaussian curve
q_i	constant term of c_i
$q_{i,x/z}$	constant term of $c_{i,x/z}$
u_x	horizontal movement
u_z	vertical movement
$u_{x,max}$	maximum horizontal displacement
$u_{z,max}$	maximum vertical displacement
x	horizontal offset distance from tunnel centreline
x	horizontal offset distance from tunnel centreline
x^*	horizontal distances of the point where $u_z \approx 0.606 u_{z,max}$
$\partial x^*/\partial z$	change in x^* with respect to depth
x^{**}	horizontal distances of the point where $u_z \approx 0.303 u_{z,max}$
$\partial x^{**}/\partial z$	change in x^{**} with respect to depth
z	depth, measured from ground surface
z_t	depth of tunnel axis
C	cover
D	tunnel diameter
I_d	soil relative density
K	trough width parameter based on i
K^*	trough width parameter based on x^*
K^{**}	trough width parameter based on x^{**}

M^*, $K_{s,Vlt}^{*slope,ln}$, $K_{s,Vlt}^{*int,ln}$	parameters of K^*
M^{**}, $K_{s,Vlt}^{**slope,ln}$, $K_{s,Vlt}^{**int,ln}$	parameters K^{**}
K_s, K_s^*, K_s^*	trough width parameters at the surface
N	centrifuge acceleration scale factor
R	tunnel radius
$V_{l,s}$	volume loss of soil
$V_{l,t}$	volume loss of tunnel
V_0	tunnel cross-sectional area
ΔV	tunnel ground loss
α	compressibility term
β	parameter used to normalise $V_{l,s}$ with C/D
ε	convergence parameter
ε_0	equivalent ground loss parameter
$\varepsilon_{x,z}$	modified equivalent ground loss parameter
δ	ovalization parameter
λ	parameter of $V_{l,t}$ in the empirical formulas for $V_{l,s}$
ν	Poisson's ratio of the soil
ρ	relative distortion parameter
ξ	empirical corrective term of semi-analytical solutions
ξ_x	empirical corrective term in the horizontal direction
ξ_z	empirical corrective term in the vertical direction
ξ^*	ratio between total experimental and elastic displacements
$\xi_{x,z}^*$	ratio between horizontal/vertical experimental and elastic displacements
EL	Elastic
EMP	Empirical
EMP-sG	Empirical method based on the standard Gaussian curve
EMP-mG	Empirical method based on the modified Gaussian curve
EXP	Experimental
SA	Semi-analytical

implemented in numerical and analytical studies of tunnel-structure interaction, especially when horizontal ground displacements significantly affect the response of the system (Basile, 2014; Dias and Bezuijen, 2017; Haji et al., 2018a; Huang and Mu, 2012; Kitiyodom et al., 2005; Franza et al., 2017; Mu et al., 2012; Zhang et al., 2011, 2013), whereas empirical methods have been used for tunnel-structure interaction in the case of buildings, tunnels, and pipelines (Basmaji et al., 2017; Klar et al., 2007; Klar and Marshall, 2008, 2015; Li et al., 2015; Son, 2015, 2016; Yu et al., 2013). These soil-structure interaction analyses are useful within design or risk assessment procedures, where the greenfield displacement input can be decided based on the specific scenario under consideration.

2. Scope of work and applicability of results

This paper presents two efficient methods that allow the replication of greenfield tunnelling-induced ground movements measured from centrifuge tests in sand. Experimental centrifuge test data (labelled in the paper as 'EXP') were obtained using a water-filled flexible membrane model tunnel, as reported in Marshall et al. (2012) and Franza et al. (in press). Empirical (labelled as 'EMP') methods developed by previous researchers are modified to improve the calculation of settlement trough characteristics (i.e. vertical movement only) and incorporate the effects of soil relative density. Then, semi-analytical (labelled as 'SA') formulas are proposed for both horizontal and vertical ground movements. Semi-analytical results are first compared against experimental data to evaluate the accuracy of the method. Subsequently, the predictions of the proposed semi-analytical methods are compared against solutions, available in the literature, of displacements for undrained clay to demonstrate the differences that occur when tunnelling in clay and sand.

The proposed empirical and semi-analytical formulas could be useful within soil-structure interaction analyses of centrifuge tests with comparable conditions, where an input of greenfield ground movements is required (e.g. Farrell et al., 2014; Franza et al., 2018; Klar et al., 2015; Lee and Chiang, 2007; Ritter et al., 2017). Once verified/calibrated using centrifuge test outcomes, the developed soil-structure interaction analysis methods could then be more widely applied to real tunnelling cases. This paper does not attempt to directly relate outcomes from the centrifuge tests to field cases; the context of the paper focuses on centrifuge studies of tunnelling problems in sand.

3. Background

3.1. The concept of volume loss, its magnitude and distribution

Volume loss relates the magnitude of movements that occur as a result of tunnelling. Soil volume loss, $V_{l,s}$, is defined as the ratio between the volume of the settlement trough per unit length of tunnel, V_s, and the final tunnel cross-sectional area, V_0. Tunnel volume loss, $V_{l,t}$, is the ratio between the ground loss at the tunnel periphery, ΔV, and V_0. The relationship between $V_{l,t}$ and $V_{l,s}$ is affected by ground conditions through the influence of volumetric strains (Marshall et al., 2012; Franza et al., in press). These volume losses are sketched in Fig. 1(a). Note that $V_{l,t}$ is a controlled variable for experimental, analytical and numerical studies, whereas it is back-calculated in the field from ground movements.

The assumed ground loss shape at the tunnel periphery plays an important role when modelling tunnel excavation. Some analytical approaches assume a uniform convergence around the tunnel boundary, however this assumption does not describe actual conditions adequately. Centrifuge modelling has confirmed that little ground
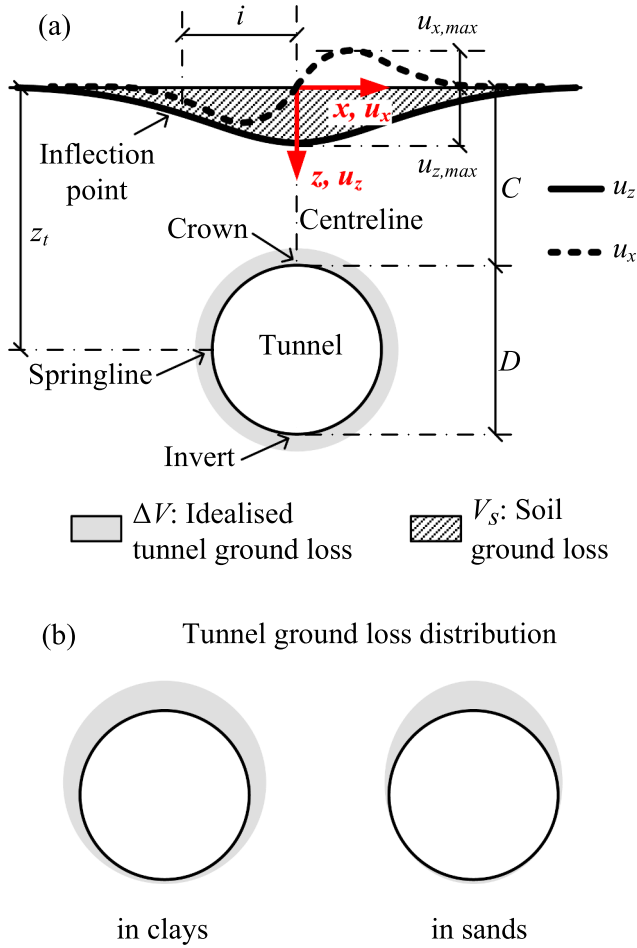
Fig. 1. (a) Illustration of soil and tunnel ground losses; (b) typical tunnel ground loss distributions for shallow tunnels.

displacement occurs at the tunnel invert for shallow tunnels (Mair, 1979; Potts, 1976). The actual tunnel ground loss is distributed according to a roughly elliptical shape in clays (Rowe and Kack, 1983; Loganathan and Poulos, 1998), whereas the ground loss is concentrated at the tunnel crown in sands (Marshall, 2009; Zhou, 2014) (see Fig. 1(b)). Several methods are available to estimate ground loss at the tunnel, including the empirical envelopes given by Dimmock and Mair (2007), the cavity-contraction solutions proposed by Mair and Taylor (1993) and Mo and Yu (2017), the gap parameter from Lee et al. (1992), or the theoretical study of Vu et al. (2016).

3.2. Empirical methods

Greenfield tunnelling-induced settlements, u_z, are often described using a standard Gaussian distribution which includes the maximum settlement, $u_{z,max}$, and the horizontal distance from the tunnel centreline to the inflection point of the curve, i:

$$u_z = u_{z,max}\exp\left(-\frac{x^2}{2i^2}\right) \tag{1}$$

where i can be related to the vertical distance between the tunnel axis depth, z_t, and the depth of interest, z, through the trough width parameter K:

$$i = K(z_t - z) \tag{2}$$

For the soil above a new tunnel, Mair et al. (1993) related the parameter K to the relative depth z/z_t as follows

$$K = \frac{K_s + (\partial i/\partial z)(z/z_t)}{1 - z/z_t} \tag{3}$$

where K_s is the value of K at the surface, and $(\partial i/\partial z)$ is the slope of i with depth when all other parameters are kept constant. For clays, Mair et al. (1993) suggested $K_s = 0.5$ and $(\partial i/\partial z) = -0.325$. On the other hand, for sands and gravels Mair and Taylor (1997) reported a significant scatter in the available data for K_s, with values ranging from 0.25 to 0.45. Based on a regression analysis of field data, Jones (2010) proposed a logarithmic formula for the prediction of K in clays that depends on the height above the tunnel $z_t - z$ rather than the relative depth z/z_t.

The modified Gaussian curve can better represent settlements induced by shallow tunnels in sandy soils (Vorster et al., 2005):

$$u_z = u_{z,max}\frac{n}{(n-1) + \exp[a(x/i)^2]}$$
$$n = e^{a\frac{2a-1}{2a+1}} + 1 \tag{4}$$

where a is an additional fitting parameter with respect to the standard Gaussian curve. Studies have illustrated that the width parameter i in sands increases with the cover to diameter ratio, C/D, (Cover, $C = z_t - D/2$, where D is tunnel diameter) and decreases with the magnitude of tunnel volume loss, $V_{l,t}$ (Marshall et al., 2012; Sugiyama et al., 1999; Zhou et al., 2014).

The modified Gaussian curve is more versatile than the standard Gaussian curve, however the additional fitting parameter, a, does not have a physical meaning. Therefore, Marshall et al. (2012) suggested to characterise the shape of any empirical curve with three degrees of freedom, including the modified Gaussian curve, by the offsets x^* and x^{**} corresponding to the points $[x^*, u_{z,max}/\sqrt{e}]$ and $[x^{**}, u_{z,max}/(2\sqrt{e})]$, where $u_{z,max}/\sqrt{e}$ is the settlement at the inflection point of the standard Gaussian curve (i.e. if $a = 0.5$, $x^* = i$). Therefore, x^* and x^{**} are the horizontal distances between the tunnel centreline and the point where $u_z \approx 0.606u_{z,max}$ and $u_z \approx 0.303u_{z,max}$, respectively. In their empirical approach, x^* and x^{**} were related to the depth of interest, z, through

$$x^* = K^*(z_t - z)$$
$$x^{**} = K^{**}(z_t - z) \tag{5}$$

To predict the change in settlement trough shape that occurs in dense sands as tunnel volume loss increases for varying C/D ratios, Marshall et al. (2012) proposed the following equations:

$$K^* = \frac{K_s^* + (\partial x^*/\partial z)(z/z_t)}{1 - z/z_t}$$
$$K^{**} = \frac{K_s^{**} + (\partial x^{**}/\partial z)(z/z_t)}{1 - z/z_t} \tag{6}$$

$$K_s^* = K_{s,Vlt}^{*int} + K_{s,Vlt}^{*slope} V_{l,t}$$
$$K_s^{**} = K_{s,Vlt}^{**int} + K_{s,Vlt}^{**slope} V_{l,t} \tag{7}$$

where
$K_{s,Vlt}^{*int} = 0.44 + 0.055C/D$, $K_{s,Vlt}^{*slope} = -0.041$, $(\partial x^*/\partial z) = -0.436$, K_s^{**}, and
$= K_s^* + 0.29$
$(\partial x^{**}/\partial z) = (\partial x^*/\partial z) - 0.20$. Note that these expressions were obtained based on a regression of centrifuge data that assumed a linear variation of the trough shape parameters with tunnel volume loss and C/D ratio.

To assess the relationship between $V_{l,s}$ and $V_{l,t}$ at the surface, Marshall et al. (2012) proposed the use of an empirical formula valid for dense sands (relative density $I_d = 90\%$) and $C/D = 1.3 - 4.4$, which can be modified into the following form by considering that the relationship should have an intercept equal to zero (i.e. $V_{l,s} = 0$ for $V_{l,t} = 0$):

$$\frac{V_{l,s}^{exp}}{(C/D)^\beta} = c_b\left(\exp\left[-\frac{c_c^2}{c_d^2}\right] - \exp\left[-\left(\frac{V_{l,t} + c_c}{c_d}\right)^2\right]\right) \tag{8}$$

where the c coefficients depend on the type of sandy soil and its relative density. For dry dense silica sand, Marshall et al. (2012) proposed

$c_b = 3.7$, $c_c = 2.8$, $c_d = 3.6$, and $\beta = 0.5$.

In the Appendix, the complete framework is provided to illustrate how settlement trough shape can be predicted using modified Gaussian curves. In particular, Eq. (26) relates the degrees of freedom of the modified Gaussian curve defined in Eq. (4) (a, i, $u_{z,max}$) to the parameters of the empirical method (K^*, K^{**}, $V_{l,s}$). This framework, which has not been detailed before, is needed to be able to use the modified Gaussian based empirical method. Note that the empirical method parameters (K^*, K^{**}, $V_{l,s}$) may be related to any generic empirical curve with three degrees of freedom (e.g. the yield density curve from Celestino et al., 2000).

3.3. Analytical solutions

Analytical solutions solve for ground displacements based on an assumed displacement pattern at the tunnel periphery (uniform convergence, ovalization, vertical translation, as shown in Fig. 2, including the positive sign convention). This approach relies on the fact that far-field ground movements (i.e. at some distance from the tunnel periphery) depend predominately on the ground loss distribution around the tunnel (González and Sagaseta, 2001). There are two components of tunnel deformation: uniform convergence and ovalization. The tunnel volume loss is related to the convergence parameter ε as

$$V_{l,t} = \frac{\Delta V}{V_0} \times 100 \approx \frac{2\pi R u_\varepsilon}{\pi R^2} \times 100 = 2\varepsilon \times 100 \tag{9}$$

whereas the ovalization mechanism is not associated with tunnel ground loss.

3.3.1. Elastic solution for deep tunnels

For deep tunnels, it is legitimate to neglect the influence of the free surface. The problem of evaluating the displacements due to the excavation of a circular tunnel within an infinite isotropic elastic medium was solved by Pender (1980) for the excavation of a cavity in a pre-stressed medium for anisotropic initial stresses.

Within an infinite space, changes in the volumetric stress produce a uniform convergence of the tunnel periphery, u_ε, and changes in the deviatoric stress (which are not associated with tunnel volumetric changes) induce an ovalization, $u_{\delta,max}$, as shown in Fig. 2. These displacements may be normalised by the tunnel radius, R, to define the tunnel deformation components $\varepsilon = u_\varepsilon/R$ and $\delta = u_{\delta,max}/R$. As an alternative, the relative distortion parameter $\rho = \delta/\varepsilon$ can be used. For deep tunnels, the parameters for convergence, ε, and ovalization, δ, relate only to the soil elastic parameters and the initial stresses.

3.3.2. Elastic solutions for shallow tunnels

A number of studies have investigated the application of the superposition of singularities method to the problem of tunnelling-induced ground displacements in a half-space. For this approach, ε and δ are considered as input parameters regardless of their relationship to soil and tunnel parameters. Their values are generally obtained by back-analysis and curve-fitting of field measurements and may not reflect realistic conditions.

The first application of the superposition of singularities method was proposed by Sagaseta (1987) to evaluate soil movements in undrained conditions. It was assumed that a shallow void of radius R_v (whose area represents the tunnel volume loss, $\Delta V = \pi R_v^2$) and located within a half-space at depth z_t is created and filled by the surrounding incompressible (Poisson's ratio $\nu = 0.5$), linear, and isotropic soil. Verruijt and Booker (1996) used the equations of Pender (1980) within the superposition of singularities method to account for ground compressibility (through Poisson's ratio) and the tunnel ovalization deformation mechanism. In the superposition of singularities method, the input deformation parameters, ε and δ, do not induce perfect uniform contraction and ovalization of the tunnel in the half-space scenario (as they would in the full-space) due to the influence of the surface. As discussed by Pinto and Whittle (2006), this aspect is often not correctly accounted for by researchers.

Exact solutions of movements induced by ground loss, ovalization and buoyancy (due to the self-weight of the removed soil) in the elastic half-space have been obtained by using the complex variable method (Fu et al., 2016; Verruijt, 1997; Strack and Verruijt, 2002; Verruijt and Strack, 2008; Zhang et al., 2018). However, the superposition of singularity method provides a sufficiently accurate approximation of the exact solution in the case of ground loss and tunnel ovalization (especially for $C/D > 2$) (Pinto et al., 2014).

Elastic solutions can adequately match surface and subsurface greenfield deformation patterns measured in the field for clays (Ieronymaki et al., 2016, 2018; Pinto et al., 2014). However, the elastic approach of Verruijt and Booker (1996) over-predicts the horizontal and vertical settlements in the far field, particularly for low ovalization terms, with wider troughs and larger horizontal movements than observed in the field (Loganathan and Poulos, 1998).

3.3.3. Elastoplastic solutions for shallow tunnels

González and Sagaseta (2001) modified the Verruijt and Booker (1996) elastic solution for an incompressible medium ($\nu = 0.5$) to account for the effect of soil volumetric behaviour by means of a compressibility term α. They introduced α based on the fact that, in a non-elastic medium, the displacements attenuate with a power law that relates to the distance within the plastic zone, $O(1/r^\alpha)$. The compressibility parameter α should be assumed equal to the mean value within the soil; α is lower or greater than unity for an overall compressive or dilative behaviour of the soil, respectively. For $\alpha = 1$, the elastic solution of Verruijt and Booker (1996) for the incompressible medium is obtained.

The efficiency of the closed-form solution provided by González and Sagaseta (2001) was assessed against centrifuge data by Franza and
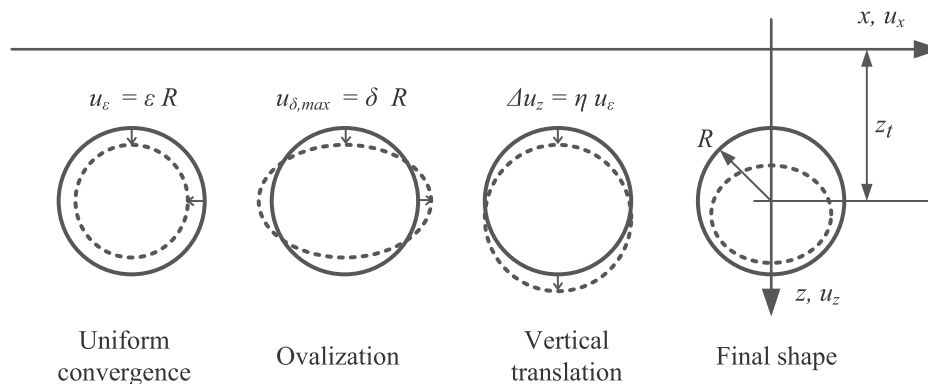
Fig. 2. Tunnel displacement components after González and Sagaseta (2001).

Marshall (2015a). Rather than calibrating the input deformation parameters predominately at the ground surface based on sparse sets of data (e.g. González and Sagaseta, 2001; Pinto et al., 2014; Ieronymaki et al., 2016), the value of $\rho = 1$ was used to give the correct representation of the centrifuge model tunnel deformation mechanism (as shown in Fig. 1(b)) and a compressibility parameter $\alpha = 0.9 - 1.3$ was adopted to reflect the relationship between $V_{l,s}$ and $V_{l,t}$ in the centrifuge tests, which were done in dry dense silica sand.

Fig. 3 displays the effects of the ovalization term and the compressibility parameter on the normalised surface settlement trough. According to Franza et al. (in press), the value of i in sandy soils decreases with tunnel volume loss from values of approximately $(0.5 - 0.7)z_t$ to $(0.35 - 0.5)z_t$ (depending also on the relative tunnel depth). This range is represented in Fig. 3 by the grey shaded areas and lines 1–3. Comparing the $\rho = 1$ line (which is physically appropriate) with the Gaussian curves in Fig. 3a shows that this input provides an analytical surface settlement trough that is too wide, especially nearer the surface. Using a higher value of ρ (as in Fig. 3(a)) or α (as in Fig. 3(b)) can give a better match to the shape of the Gaussian curve, however this would not be realistic when considering the physical meaning of the parameters. In addition, using $\rho = 1$ with average values of α representative of the entire ground mass does not provide good predictions of subsurface ground movements when compared against measurements from centrifuge tests (Franza and Marshall, 2015a).

3.4. Semi-analytical solutions

Semi-analytical solutions have been developed by applying an empirical corrective term, ξ, to displacement patterns from elastic solutions, u^{el}, such that the semi-analytical displacement field is $u^{sa} = \xi u^{el}$. Loganathan and Poulos (1998) proposed the evaluation of vertical and horizontal undrained movements in clays based on the elastic solution of Verruijt and Booker (1996) using an ovalization term $\delta = 0$ and by substituting the modified equivalent ground loss parameter $\varepsilon_{x,z}$ to ε:

$$\varepsilon_{x,z} = \xi\varepsilon = \varepsilon_0\exp\left[-\left(\frac{1.38x^2}{(z_t+R)^2} + \frac{0.69z^2}{z_t^2}\right)\right]$$

$$\xi = 2\exp\left[-\left(\frac{1.38x^2}{(z_t+R)^2} + \frac{0.69z^2}{z_t^2}\right)\right] \tag{10}$$

where R is the tunnel radius, z_t is the depth to the tunnel axis, x is the distance from the tunnel centreline, z is depth, ν is the Poisson's ratio of the soil, $\varepsilon_0 = V_{l,t}/100$ is the equivalent ground loss parameter. As discussed by Pinto and Whittle (2006), the provided $\varepsilon_{x,z}$ is the outcome of a calibration process in which the corrective term ξ was conveniently chosen to account for field observations and centrifuge model test outcomes.

4. Centrifuge data of greenfield tunnelling

Empirical and semi-analytical methods are used in this paper to replicate results from the centrifuge tests of plane-strain tunnelling presented by Marshall et al. (2012) and Franza et al. (in press), which compile data from Marshall (2009), Farrell (2010), Zhou (2014), Franza (2016).

The centrifuge models included a strong box, soil, model tunnel, and a tunnel volume control system (Fig. 4 shows the set-up used by Marshall (2009); refer to Marshall (2009), Zhou (2014), Franza (2016) for full details). All tests used a dry silica sand known as Leighton Buzzard Fraction E. The model tunnel comprised a metallic cylinder with enlarged ends which was covered by a latex sleeve and filled with water. The plane-strain centrifuge strongboxes consisted of a U-channel, a Perspex front wall, and a metallic back wall. The tunnel volume loss $V_{l,t}$ was induced by extracting water from the model tunnel using a volume control system: a constant-head standpipe, a solenoid valve, a linear actuator, a water-filled sealed cylinder and a linear variable differential transformer were used to (1) compensate, during centrifuge spin-up from $5g$ to Ng (where g is gravity and N is the centrifuge acceleration scale factor), for volume loss within the system due to the compressibility of air trapped within the water; (2) upon reaching the target Ng-level, extract a specific volume of water from the tunnel, replicating the tunnel volume loss $V_{l,t}$. The transparent Perspex wall allowed for digital images to be taken at each increment of $V_{l,t}$ for subsequent analysis using GeoPIV (White et al., 2003) to determine subsurface ground movements.

Tests included soil with relative density (I_d) of 30% (loose), 50% (medium-dense), and 90% (dense), and cover-to-diameter ratios (C/D) of 1.3, 2.4, 4.4, and 6.3. Table 1 summarises the geometry and soil density of the performed tests, including the adopted Ng level of each test. Tests are labelled according to their C/D ratio and I_d (i.e. a test with $C/D = 6.3$ and $I_d = 0.9$ is labelled CD6.3ID90). Centrifuge tests were carried out using model tunnels with varying diameter. Thus, in this paper, centrifuge data are normalised with respect to the tunnel radius R. Importantly, regression analyses of empirical and semi-analytical expressions are limited to the range $V_{l,t} = 0 - 5\%$.

5. Empirical methods for vertical ground movements

5.1. Trough width - existing methods for settlements in dense sand

The empirical approach of Marshall et al. (2012) was developed based on data from experiments in dense sand and C/D between 1.3 and 4.4. To investigate the effects of high C/D values, Franza et al. (2016) performed regression analyses of K^* and K^{**} for dense sand (tests CD1.3ID90, CD2.0ID90, CD2.4ID90, CD4.4ID90, and CD6.3ID90); data were curve-fitted with the surface described by Eqs. (6) and (7) proposed by Marshall et al. (2012) and scalar values of the six trough shape
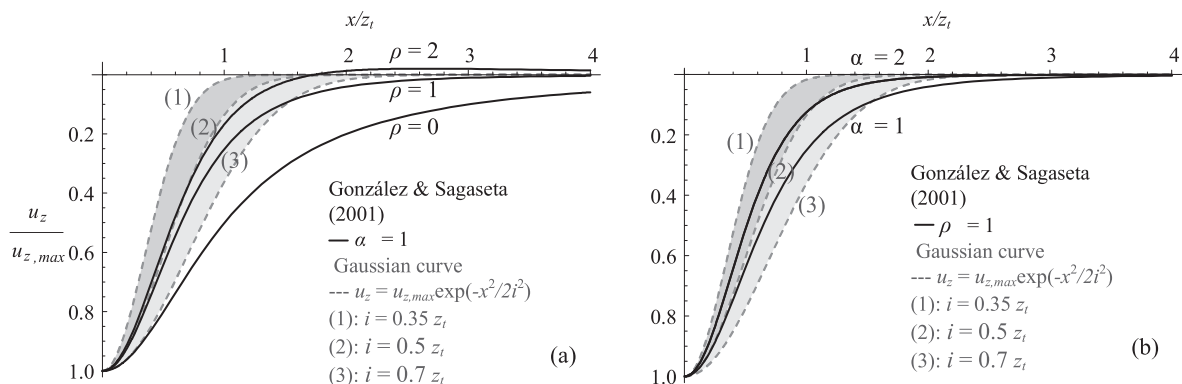

Fig. 3. Normalised analytical surface settlement trough: effects of (a) tunnel ovalization and (b) ground compressibility (Franza and Marshall, 2015a).
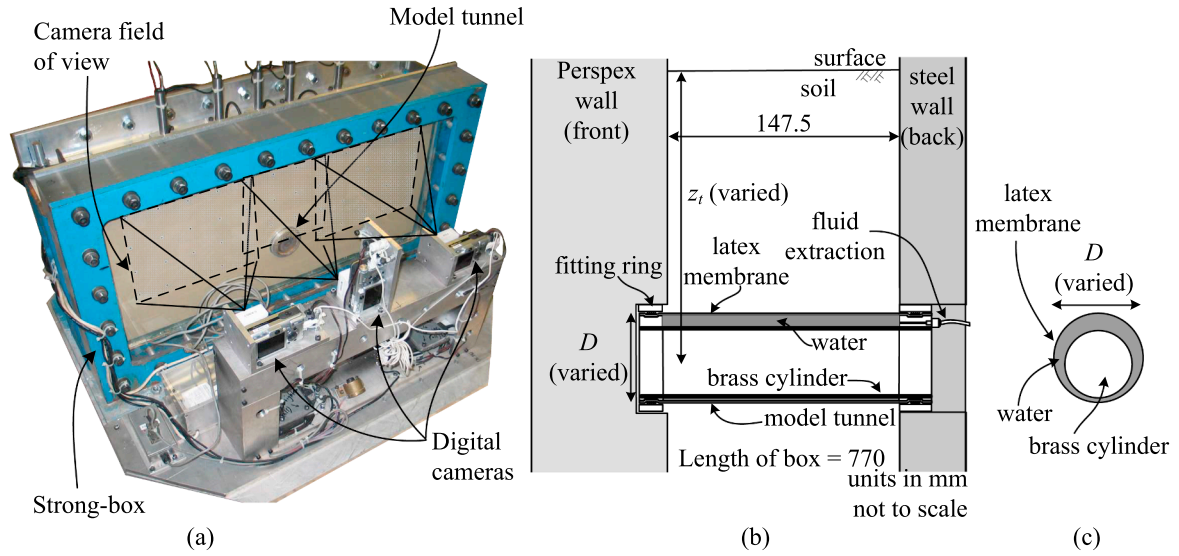
Fig. 4. Set-up from Marshall et al. (2012): (a) model package; (b) cross-section through model (units mm; not to scale); (c) cross-section through tunnel.

Table 1
Summary of centrifuge tests for greenfield tunnelling in model scale dimensions (Franza et al., in press).

Name[b]	D (mm) [m][a]	z_t (mm) [m][a]	C/D (–)	I_d (%)	N (–)
CD1.3ID30(F)	90 [7.20]	165 [13.20]	1.3	30	80
CD1.3ID50(F)	90 [6.30]	165 [11.60]	1.3	50	70
CD1.3ID90(M)	82 [6.15]	150 [11.30]	1.3	90	75
CD2.0ID30(F)	90 [7.20]	225 [18.00]	2.0	30	80
CD2.0ID50(Z)	90 [7.20]	225 [18.00]	2.0	50	80
CD2.0ID70(Z)	90 [7.20]	225 [18.00]	2.0	70	80
CD2.0ID90(Z)	90 [7.20]	225 [18.00]	2.0	90	80
CD2.5ID30(F)	90 [7.20]	270 [21.60]	2.5	30	80
CD2.4ID90(M)	62 [4.65]	182 [13.70]	2.4	90	75
CD4.5ID30(F)	40 [3.20]	200 [16.00]	4.5	30	80
CD4.5ID50(F)	40 [3.20]	200 [16.00]	4.5	50	80
CD4.4ID90(M)	60 [2.40]	295 [11.80]	4.4	90	40
CD6.3ID30(F)	40 [3.20]	270 [21.60]	6.3	30	80
CD6.3ID50(F)	40 [3.20]	270 [21.60]	6.3	50	80
CD6.3ID90(F)	40 [3.20]	270 [21.60]	6.3	90	80

[a] Prototype scale dimension in square brackets.
[b] Group in brackets. F: Franza (2016); Zhou (2014); M: Marshall et al. (2012)

parameters $(K_{s,Vlt}^{*int}, K_{s,Vlt}^{*slope}, K_s^*, K_s^{**}, (\partial x^*/\partial z), (\partial x^{**}/\partial z))$ were obtained. Franza et al. (2016) showed that the variation of these six shape parameters with C/D has a non-linear trend due to a transition between shallow and deep tunnels. Franza et al. (2016) applied a regression of

the trough shape parameter coefficients with C/D based on logarithmic expressions (similar to Jones (2010) for clays). The resulting set of equations from this regression analysis are given by:

$$\partial x^*/\partial z = -0.094\ln[C/D] - 0.378;$$
$$\partial x^{**}/\partial z = -0.064\ln[C/D] - 0.712$$
$$K_{s,Vlt}^{*slope} = +0.005\ln[C/D] - 0.040;$$
$$K_{s,Vlt}^{**slope} = +0.016\ln[C/D] - 0.070$$
$$K_{s,Vlt}^{*int} = +0.180\ln[C/D] + 0.424;$$
$$K_{s,Vlt}^{**int} = +0.255\ln[C/D] + 0.779 \tag{11}$$

Results obtained using Eqs. (6), (7) and (11) are compared against the centrifuge measurements of K^* and K^{**} in Fig. 5 for $V_{l,t} = 1$ and 5% and $z/z_t = 0 - 0.7$ (the supplemental data has a figure which includes $V_{l,t} = 2.5\%$). Results compare well with most of the data used in the statistical regression presented by Franza et al. (2016) (limited to $I_d = 0.9$). On the other hand, Fig. 5(a) shows that the comparison is less good for test CD1.3ID90, especially at high volume losses and greater depths. This is because the empirical expressions give a qualitatively different trend of the width parameters with depth, which results in predicted values of K^* and K^{**} being significantly lower than the experimentally obtained values (and close to an unrealistic value of zero for K^* at greater depths). Similar results were obtained at low C/D values by Marshall et al. (2012), who assumed a linear variation of the trough shape parameters. In the next section, a new set of equations is
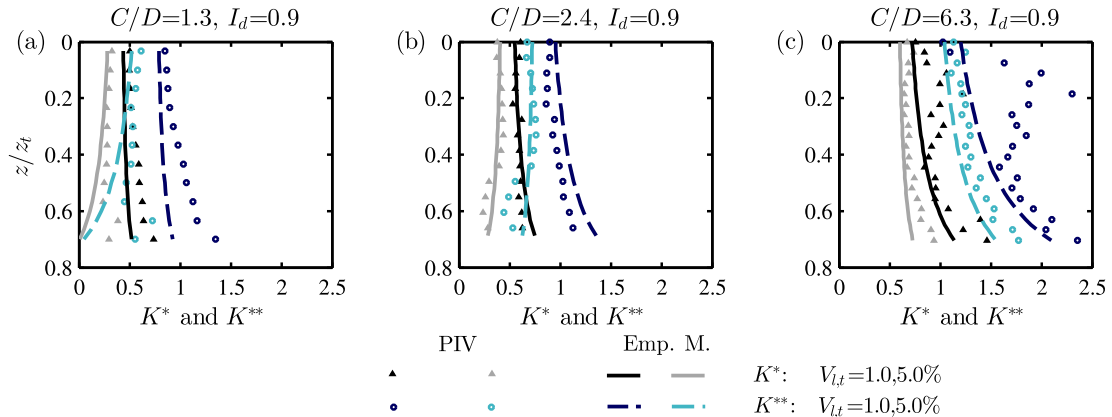

Fig. 5. Trough width parameters: experimental data versus predictions obtained using Eqs. (6), (7) and (11).

presented that overcomes this issue at low C/D and that also accounts for the effect of soil relative density.

5.2. Trough width - new approach for settlements in sand with varying relative density

A new approach is proposed to assess settlement trough width parameters, K^* and K^{**}, as a function of I_d, C/D, $V_{l,t}$, and z/z_t, based on Eq. (6). To improve performance, the non-linear trends of x^*, x^{**}, K_s^*, and K_s^{**} illustrated by Franza (2016) are accounted for in Eq. (12) with logarithmic functions (e.g. the partial derivatives of x^* and x^{**} were obtained assuming a logarithmic trend of x^* and x^{**} with $1 + z/z_t$).

$$K_s^* = K_{s,Vlt}^{*int,ln} + K_{s,Vlt}^{*slope,ln}\ln[V_{l,t} + 1]$$
$$K_s^{**} = K_{s,Vlt}^{**int,ln} + K_{s,Vlt}^{**slope,ln}\ln[V_{l,t} + 1]$$
$$\frac{\partial x^*}{\partial z} = \frac{M^*}{1 + z/z_t}; \qquad \frac{\partial x^{**}}{\partial z} = \frac{M^{**}}{1 + z/z_t} \tag{12}$$

Eqs. (6) and (12) have six coefficients ($M^*;M^{**};K_{s,Vlt}^{*slope,ln};K_{s,Vlt}^{**slope,ln};K_{s,Vlt}^{*int,ln};K_{s,Vlt}^{**int,ln}$) that are dependant on the variables C/D and I_d.

The values of these coefficients were defined based on a regression analysis including the entire dataset of tests (groups F, M, Z) for $V_{l,t} = 0.5 - 5\%$ and $z/z_t = 0 - 0.7$. The obtained regression analysis results are shown as markers in Fig. 6. The plots illustrate the variation of the six coefficients of Eq. (12) with C/D for varying soil density (I_d is plotted using different colours and marker-shapes).

Based on the logarithmic reduction of width parameter coefficients with C/D due to a transition from shallow to deep tunnels, it may be assumed that

$$\kappa = g[I_d]\ln[C/D] - h[I_d] \tag{13}$$

where κ is used to indicate one of the obtained coefficients (i.e. M^*, M^{**}, $K_{s,Vlt}^{*slope,ln}$, $K_{s,Vlt}^{**slope,ln}$, $K_{s,Vlt}^{*int,ln}$, $K_{s,Vlt}^{**int,ln}$), and $g[I_d]$, $h[I_d]$ are functions of I_d. Considering that the settlement trough width decreases with soil density for relatively deep tunnels, for the sake of simplicity, the interpolation of the regression analysis results (i.e. markers in Fig. 6) with Eq. (13) was performed assuming a linear variation of the functions $g[I_d]$ and $h[I_d]$ with density. This resulted in the set of expressions in Eq. (14), which are plotted as solid lines in Fig. 6. Although this method does not account for the complex pattern of results corresponding to $C/D = 2.0$, which is due to the variation of the arching

mechanism with soil density (Franza et al., in press), overall Eq. (14) provides a good interpolation.

$$M^* = (+0.81I_d - 0.93)\ln[C/D] - 0.60I_d - 0.07$$
$$M^{**} = (+1.50I_d - 1.55)\ln[C/D] - 0.96I_d - 0.28$$
$$K_{s,Vlt}^{*slope,ln} = (+0.35I_d - 0.30)\ln[C/D] - 0.22I_d + 0.07$$
$$K_{s,Vlt}^{**slope,ln} = (+0.41I_d - 0.35)\ln[C/D] - 0.22I_d - 0.01$$
$$K_{s,Vlt}^{*int,ln} = (-0.84I_d + 0.95)\ln[C/D] + 0.45I_d + 0.07$$
$$K_{s,Vlt}^{**int,ln} = (-1.16I_d + 1.36)\ln[C/D] + 0.47I_d + 0.42$$

$$\tag{14}$$

In addition, to guarantee the physical sense of Eq. (4) as a settlement trough, the condition $K^{**} = \min[K^{**EM};1.85K^{*,EM}]$ is required to satisfy $n > 0$, where the width parameters calculated with empirical equations are indicated as $K^{*,EM}$ and $K^{**,EM}$. Further details are provided in Appendix A.

The performance of Eqs. (6), (12) and (14) against the centrifuge measurements of K^* and K^{**} is illustrated in Fig. 7 for $V_{l,t} = 1$ and 5% (the supplemental data has a figure which includes $V_{l,t} = 2.5\%$), $I_d = 0.3$ and 0.9 (loose and dense sands), and $z/z_t = 0 - 0.7$. Overall, the empirical predictions are shown to provide a satisfactory match with both K^* and K^{**}. Additionally, it can be seen that the proposed expressions are able to describe the variation of settlement trough width with soil density (which has not previously been done). Furthermore, there is a significant improvement in the prediction of subsurface values of K^* and K^{**} at $C/D = 1.3$ with the new approach (compare Figs. 5 and 7; also note that more comprehensive plots of the width parameters for $V_{l,t} = 1, 2.5, 5\%$ are available in the supplemental data). The improved performance is likely the result of the assumption of logarithmic trends of the main variables, which takes into account the fact that [i] the process of soil stiffness degradation with strains is non-linear, and [ii] the deeper the tunnel, the more the displacement mechanism close to the surface should converge towards an elastic pattern.

In summary, Eqs. (6), (12) and (14) may be used for the prediction of the centrifuge test results of surface and subsurface settlement trough shape parameters for loose, medium-dense and dense sands.

5.3. Relationship between soil and tunnel volume loss

The relationship between $V_{l,s}$ and $V_{l,t}$ is required to fully define empirical settlement curves (e.g. the standard or modified Gaussian
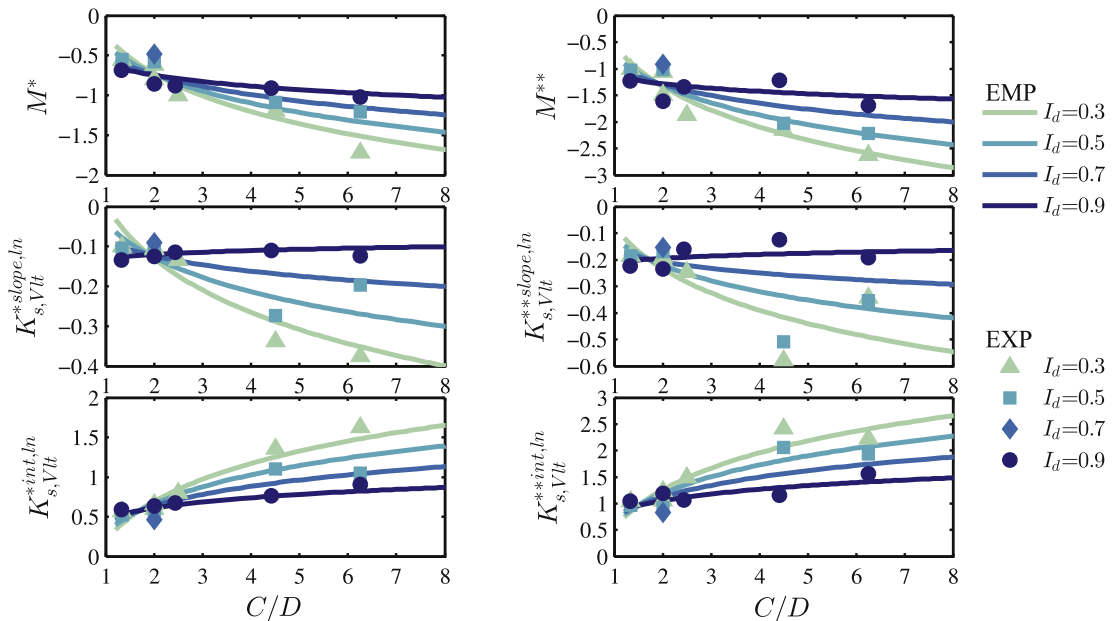

Fig. 6. Outcomes of settlement trough parameter regression using new approach for varying I_d.
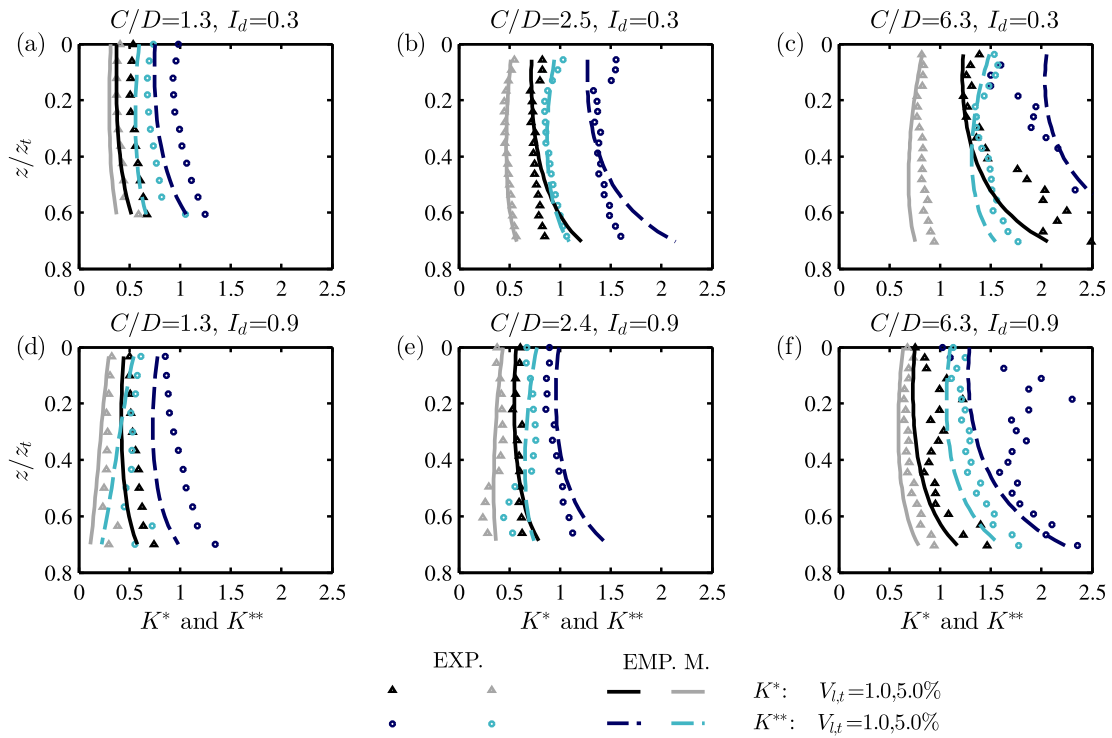
Fig. 7. K^* and K^{**} against depth for $I_d = 0.3$ and 0.9 compared with predictions using Eqs. (6), (12) and (14).

curves) at any depth. The approach defined by Eq. (8) was extended to consider the entire data set indicated in Table 1. The soil used for all tests was the same dry silica sand, hence the values of coefficients c_b, c_c, and c_d were assumed as in Eq. (8). Zhou (2014), in analysing test group Z, suggested that the coefficient β should be a linear function of relative density. Furthermore, analyses of the full data set indicated that, for loose samples, the description of the experimental $V_{l,s}$ versus $V_{l,t}$ curves required an additional coefficient, λ, for $V_{l,t}$.

A regression analysis of data corresponding to the normalised depths $z/z_t = 0$, 0.25 and 0.5 within the range $V_{l,t} = 0 - 5\%$ resulted in Eq. (15), which accounts for both C/D and I_d. The parameters λ and β were assumed to be polynomial functions of C/D and I_d.

$$\frac{V_{l,s}^{exp}}{(C/D)^{\beta}} = 2.02 - 3.7\exp\left[-\left(\frac{\lambda V_{l,t} + 2.8}{3.6}\right)^2\right]$$

$$\begin{cases} \beta = 2.81 - 1.99 I_d - 0.38 C/D + 0.12 I_d C/D + 0.035 (C/D)^2 \\ \lambda = 0.88 + 0.51 I_d - 0.12 C/D \quad \text{if} z/z_t = 0 \end{cases}$$

$$\begin{cases} \beta = 2.55 - 1.82 I_d - 0.36 C/D + 0.09 I_d C/D + 0.037 (C/D)^2 \\ \lambda = 0.83 + 0.57 I_d - 0.12 C/D \quad \text{if} z/z_t = 0.25 \end{cases}$$

$$\begin{cases} \beta = 2.14 - 1.52 I_d - 0.29 C/D + 0.03 I_d C/D + 0.037 (C/D)^2 \\ \lambda = 0.79 + 0.53 I_d - 0.12 C/D \quad \text{if} z/z_t = 0.50 \end{cases} \quad (15)$$

These empirical expressions give quantitative guidance on subsurface soil volume losses, which has not been previously provided.

As displayed in Fig. 8, the predicted $V_{l,s}$ versus $V_{l,t}$ values (markers) give a good fit with experimental data (lines); the regression of the data set resulted in $R^2 = 0.98$, 0.95 and 0.94 for $z/z_t = 0$, 0.25 and 0.5, respectively. Note that Eq. (15) does not account for the effects of confining stress because the tunnel cover is normalised by its diameter. Therefore, judgement should be used before applying Eq. (15) to real scenarios which differ considerably to the prototype scenarios considered here. Plots of the soil volume loss against tunnel volume loss for
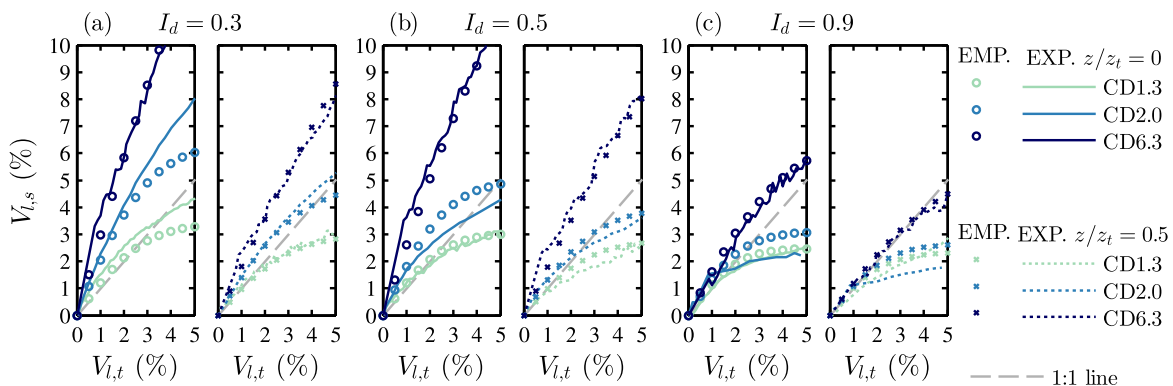

Fig. 8. $V_{l,s} - V_{l,t}$ at $z/z_t = 0$ and 0.5 compared with predictions using Eq. (15).

$C/D = 1.3, 2.0, 2.5, 4.5, 6.3$ are available in the supplemental data.

To illustrate the performance and limitations of the proposed empirical framework consisting of Eqs. (6), (12), (14) and (26), predictions (EMP-mG; solid lines) are compared against centrifuge data (EXP; markers) and a simpler (conventional) method using a standard Gaussian curve (EMP-sG; dashed lines) in Fig. 9 for $C/D \approx 1.3; 2.5; 4.5$, $z/z_t = 0; 0.5$, $V_{l,t} = 2; 5\%$, and both loose ($I_d = 0.3$) and dense ($I_d = 0.9$) sands. The width parameter at the surface for the standard Gaussian curves was taken as $K = 0.35$ (Mair and Taylor, 1997) and it was assumed that $V_{l,s} = V_{l,t}$. Results illustrate the significant influence of soil density on both the variation of settlement trough shape and the magnitude of movements. The differences between EMP-sG and EMP-mG would have important implications to the assessment of tunnel-structure interactions (e.g. in terms of maximum settlements (Mair et al., 1996), settlement trough shape (Klar et al., 2007; Giardina et al., 2015; Franza et al., 2017) or settlement trough extent (Haji et al., 2018b)).

6. Semi-analytical solution

This section presents a semi-analytical solution (SA) for the replication of the centrifuge test greenfield vertical and horizontal ground movements. The method is an extension of the work provided in Franza and Marshall (2015b) and Haji et al. (2018a) and is based on the elastic solution of Verruijt and Booker (1996), with the following details. (1) The case of an elastic medium for incompressible soil ($\nu = 0.5$) was adopted. (2) The relationship $\delta = \varepsilon$ ($\rho = 1$) was used to replicate the observed experimental tunnel deformation mechanism (centrifuge data indicate negligible u_x at the tunnel springline for $V_{l,t} = 0 - 5\%$, as shown by Franza et al. (in press)). (3) In the 'new method' introduced in this paper, two corrective terms are applied: ξ_x and ξ_z in the horizontal and vertical directions, respectively. Further details on the corrective terms are given in following sections. The semi-analytical solution for horizontal (u_x) and vertical (u_z) displacement can therefore be written as
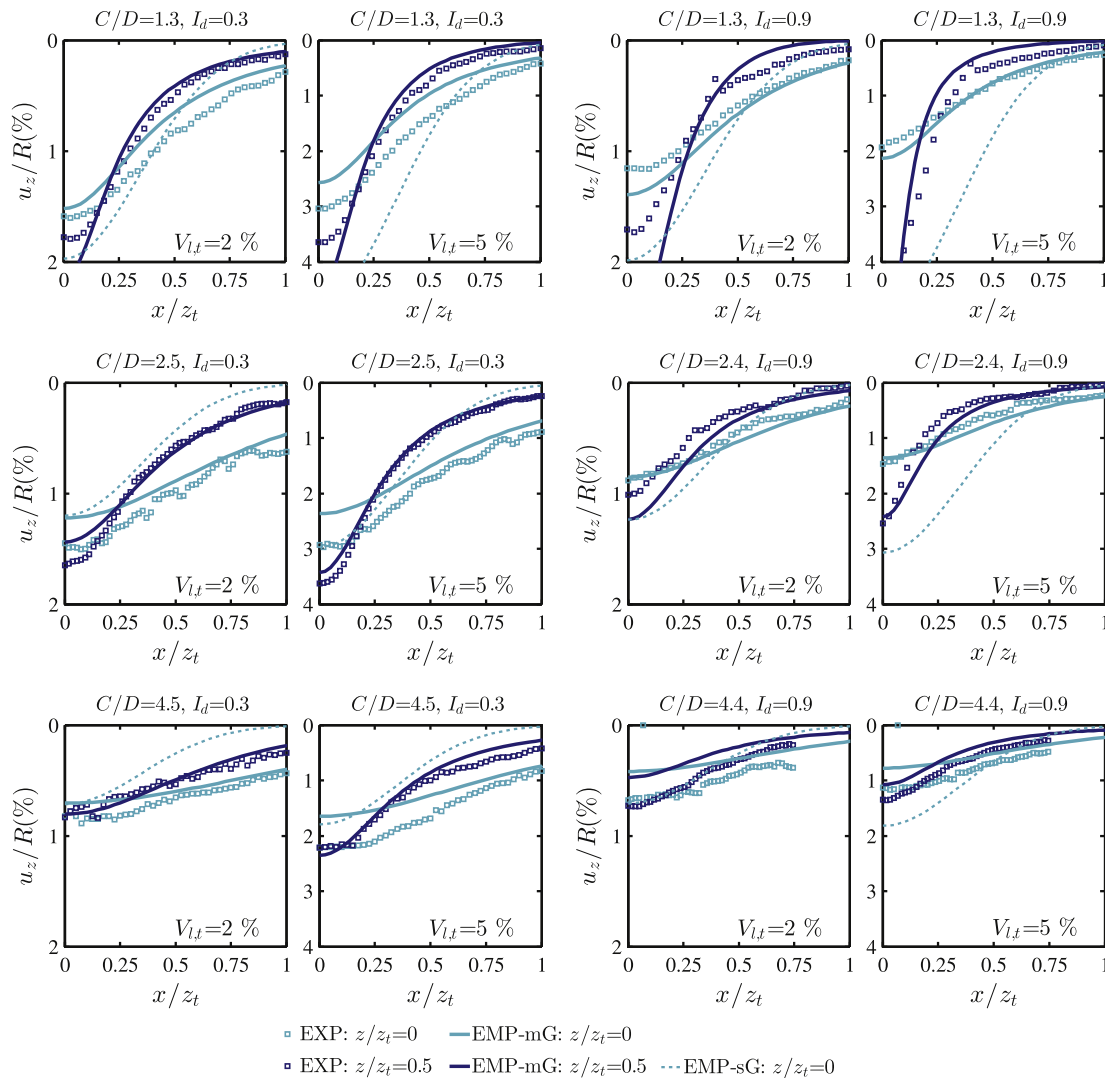

Fig. 9. Comparison between centrifuge data (EXP) and settlement troughs using modified Gaussian curves with proposed empirical formulas (EMP-mG) and conventional approach using standard Gaussian curves (EMP-sG).

$$u_x = -2\varepsilon R^2 \xi_x \left[\frac{x}{2r_1^2}\left(1 - \frac{x^2 - z_1^2}{r_1^2}\right) + \frac{x}{2r_2^2}\left(1 - \frac{x^2 - z_2^2}{r_2^2}\right) \right.$$
$$\left. - \frac{4xz}{2r_2^4}\left(z_2 - \frac{z_t(x^2 - 3z_2^2)}{r_2^2}\right) \right] \qquad (16)$$

$$u_z = -2\varepsilon R^2 \xi_z \left[\frac{z_1}{2r_1^2}\left(1 - \frac{x^2 - z_1^2}{r_1^2}\right) - \frac{z_2}{2r_2^2}\left(1 + \frac{x^2 - z_2^2}{r_2^2}\right) \right.$$
$$\left. + \frac{1}{2r_2^4}\left(2(z + z_t)(x^2 - z_2^2) + 4z_t z z_2 \frac{3x^2 - z_2^2}{r_2^2}\right) \right] \qquad (17)$$

where

$z_1 = z - z_t$, $z_2 = z + z_t$, $r_1 = \sqrt{x^2 + z_1^2}$, $r_2 = \sqrt{x^2 + z_2^2}$, $\varepsilon = V_{l,t}/(100 \times 2)$ is the tunnel convergence parameter.

An indication of the spatial distribution of the corrective terms can be obtained by plotting the ratio between the centrifuge displacement data and the elastic analytical predictions without the corrective term applied (i.e. using Eqs. (16) and (17) with $\xi_x = \xi_z = 1$). Figs. 10(a) and 11(a) display $\xi^* = u^{ex}/u^{el}$, the ratio between total (i.e. $\sqrt{u_x^2 + u_z^2}$) experimental, u^{ex}, and elastic analysis, u^{el}, ground movements. Figs. 10(b)–(c) and 11(b)–(c) plot $\xi_z^* = u_z^{ex}/u_z^{el}$ and $\xi_x^* = u_x^{ex}/u_x^{el}$ based on vertical and horizontal movements, respectively. These figures illustrate that ξ^* for the total movements is similar to the ratio of settlements ξ_z^* (compare Figs. 10(a)–(b) and 11(a)–(b)), while it differs from the ratio of horizontal movements ξ_x^* (compare Figs. 10(a)–(c) and 11(a)–(c)). For dense sands, soil arching, discussed by Franza et al. (in press), induces localised vertical and horizontal movements at the tunnel crown that impact the experimental ratios in terms of total, vertical, and horizontal movements, as shown by Fig. 10. In addition, soil relative density results in significant differences between the qualitative spatial distributions of the experimental ratios (compare Figs. 10 and 11).

In the original Franza and Marshall (2015b) method, the corrective term ξ was determined based on ξ^* from a single centrifuge test data set (CD2.4ID90); thus, it was assumed $\xi = \xi_z = \xi_x$. In this paper, to account for the effects of soil relative density on the ratios ξ_z^* and ξ_x^* illustrated in Figs. 10 and 11, the semi-analytical approach uses separate corrective terms in the horizontal and vertical direction (ξ_x and ξ_z, respectively). This approach was extended to include the full data set presented in Table 1, thereby also including for the effects of cover to diameter ratio, C/D, and soil relative density, I_d.

6.1. Corrective term - original method

Franza and Marshall (2015b) used the unique value ξ shown in Eq. (18) in both the horizontal and vertical directions to replicate the distributions of ξ from centrifuge test CD2.4ID90.

$$\xi = c_A \exp\left[-\left(c_1\left(\frac{z}{z_t}\right)^2 + c_2\left(\frac{x}{z_t}\right)^2\right)\right]$$
$$+ c_B \exp\left[-\left(c_3\left(\frac{z}{z_t} - c_4\right)^2 + c_3\left(\frac{x}{z_t}\right)^2\right)\right] \qquad (18)$$

where coefficients $c_i = m_i V_{l,t} + q_i$ depend linearly on $V_{l,t}$ to describe the narrowing of the settlement trough and development of a localised zone of large displacements at the tunnel crown that occur as tunnel volume loss increases. Eq. (18) consists of two three-dimensional Gaussian functions of both spatial coordinates x and z. The first Gaussian function with coefficients c_A, c_1 and c_2 allows interpolating ξ^* at lower volume losses (Fig. 10(a); left-side). For the first Gaussian surface, c_A is the function amplitude whereas c_1 and c_2 are the attenuation factors in the x and z directions, respectively. At higher volume losses, ξ^* exhibits an

additional peak in the proximity of the tunnel crown (Fig. 10(a); right-side). To provide a good fit, an additional Gaussian function was introduced in ξ, which has its centre at $(0, c_4 H)$, amplitude c_B, and attenuation factor c_3 in both spatial directions. The accuracy of Eqs. (16)–(18) in terms of vertical displacement prediction was good, however the solutions over-predicted subsurface horizontal movements because the calibration of the corrective factors was done on the basis of total displacements. This is because the vertical movements have a larger magnitude than the horizontal movements.

6.2. Corrective term - new method

The semi-analytical approach was extended to a wider set of centrifuge data, including the effects of cover to diameter ratio, C/D, and soil relative density, I_d. The two corrective terms ξ_z and ξ_x given in Eq. (19) were implemented in the vertical and horizontal directions, respectively, with coefficients depending on I_d, C/D, and $V_{l,t}$. The need for different terms in the x and z directions was judged necessary to improve the accuracy of results in the horizontal direction compared to the 'original method'. To include for the effects of C/D and I_d while allowing for settlement troughs wider than the elastic displacement field, two additional coefficients (c_5 and c_6) were needed.
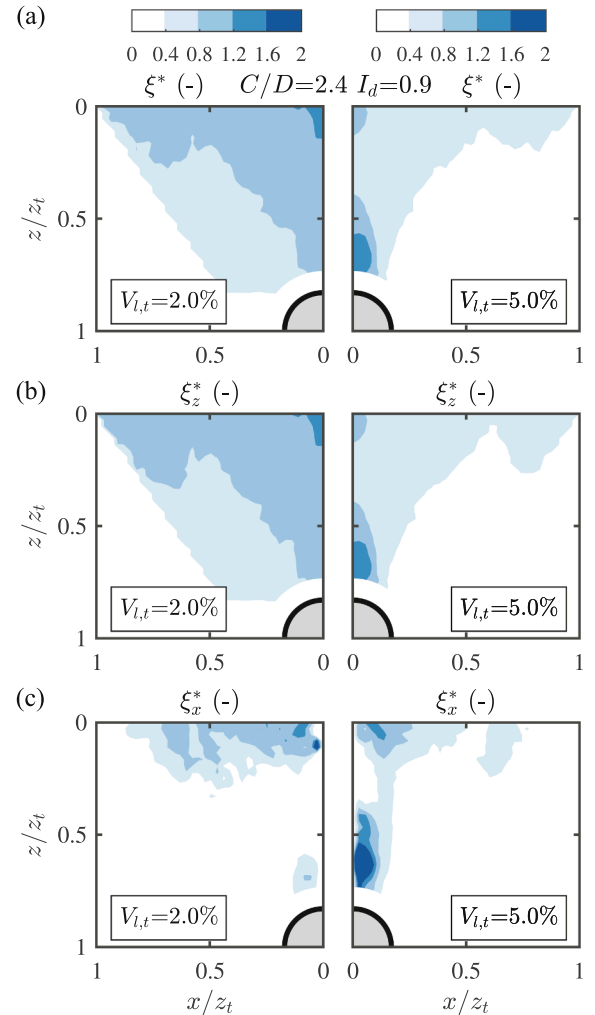

Fig. 10. Total (ξ^*), vertical (ξ_z^*), and horizontal (ξ_x^*) ratios between centrifuge and elastic displacements for CD2.4ID90.
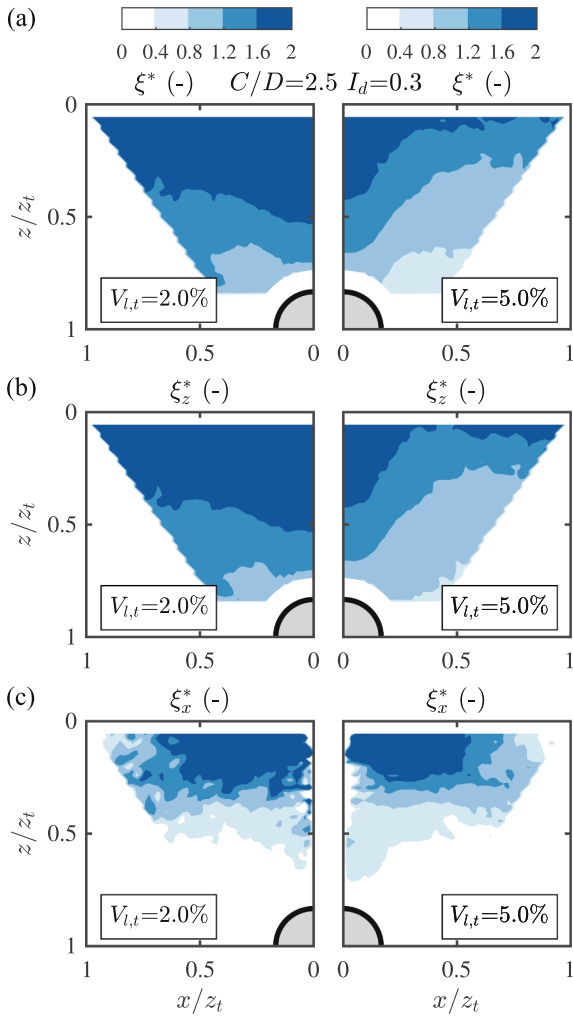
(a)

(b)

(c)

Fig. 11. Total (ξ^*), vertical (ξ_z^*), and horizontal (ξ_x^*) ratios between centrifuge and elastic displacements for CD2.5ID30.

$$
\begin{aligned}
\xi_z = \ & c_{A,z}\exp\left[-\left(c_{1,z}\left(\frac{z}{z_t}\right)^2 + c_{2,z}\left(\frac{x}{z_t}\right)^2 + c_{6,z}\left(\frac{x}{z_t}\right)^4\right)\right] \\
+ \ & c_{B,z}\exp\left[-\left(c_{3,z}\left(\frac{z}{z_t} - c_{4,z}\right)^2 + c_{5,z}\left(\frac{x}{z_t}\right)^2\right)\right] \\
\xi_x = \ & c_{A,x}\exp\left[-\left(c_{1,x}\left(\frac{z}{z_t}\right)^2 + c_{2,x}\left(\frac{x}{z_t}\right)^2 + c_{6,x}\left(\frac{x}{z_t}\right)^4\right)\right] \\
+ \ & c_{B,x}\exp\left[-\left(c_{3,x}\left(\frac{z}{z_t} - c_{4,x}\right)^2 + c_{5,x}\left(\frac{x}{z_t}\right)^2\right)\right]
\end{aligned}
\tag{19}
$$

where the coefficients c_i were determined using nonlinear data-fitting algorithms with a least-squares approach that was performed for each centrifuge test by imposing $c_i = m_i V_{l,t} + q_i$; note that $V_{l,t}$ is expressed in percentage.

The coefficients m_i and q_i, which are functions of I_d and C/D, were obtained for the entire data set of centrifuge tests (Table 1) and are listed in Appendix B. Coefficients of ξ_z were first calculated with respect to the ratio ξ^* of the total movements. Then, an additional regression was performed to optimise $c_{b,x}$, $c_{1,x}$, and $c_{2,x}$ with respect to the ratio ξ_x^* for the horizontal displacements while the remaining coefficients were kept fixed to the values obtained in the vertical direction for ξ.

It is worth noting that a regression of these coefficients with respect

to I_d and C/D was not performed because of the complex trends observed in the data. Thus, if the semi-analytical framework is to be used for intermediate values of I_d and/or C/D, it is suggested that predictions should be made using the sets of coefficients given in a row of Table 2 for the closest range of I_d and C/D, then the design displacement field can be obtained either as an averaged value of the results or by considering the envelope of the computed movements.

6.3. Comparison of semi-analytical solution predictions with centrifuge data

An indication of the accuracy of the semi-analytical formulas given by Eqs. (16), (17) and (19) (solid lines, labelled 'SA') is presented in Fig. 12 by comparing outputs with centrifuge data (markers, labelled 'EXP') from six tests with varying relative density and cover-to-diameter ratio ($I_d = 30, 90\%; C/D = 1.3, 2.5, 4.5$) for $V_{l,t} = 2, 4\%$. The displacement values were normalised by ($V_{l,t}R$) to allow comparison of data at varying volume losses and for tunnels of different sizes. In Fig. 12, the left y-axis displays the depth of the displacement profiles, while the scale of the normalised displacements is shown on the right y-axis, which differs for vertical and horizontal ground movements.

The 'new method' expressions presented here are able to replicate, with reasonable accuracy, the surface and sub-surface horizontal and vertical movements of the centrifuge data in sand as they are affected by tunnel volume loss, relative density and relative depth. The limitation of the 'original method' of Franza and Marshall (2015b), in terms of horizontal displacement prediction, was significantly improved by including the horizontal corrective term.

In addition, to illustrate the differences in tunnelling-induced displacement fields in clays and sands, the movements obtained from the semi-analytical expressions of Loganathan and Poulos (1998) for clays in undrained conditions (dashed lines, labelled 'S.A. Clay') are plotted against the 'new method' expressions (solid lines, labelled 'S.A. Sand') in Fig. 13. The soil deformation pattern in both vertical and horizontal directions for sands is significantly affected by the magnitude of tunnel volume loss, whereas it is constant with $V_{l,t}$ for clays. The differences in the settlement troughs for sands and clays are significant at depths closer to the tunnel axis, particularly at high volume losses, whereas the differences are smaller near the surface. The magnitude of horizontal displacements increases with depth in clays, whereas it decreases in sands, leading to wider subsurface horizontal movements in clays than in sands. These differences in horizontal ground movement patterns are due largely to the different tunnel ovalization mechanisms, where sandy soils have negligible inwards movement at the tunnel springline and clays have an oval-shaped tunnel contraction. These results should not be generalised to real excavations performed with tunnel boring machines that use tail-skin grouting, for which there could be outwards horizontal displacements at the tunnel periphery for large grout pressures (Bilotta and Russo, 2012; Dias and Kastner, 2013).

7. Conclusions

This paper deals with the analysis of centrifuge test data of greenfield tunnelling in sands and the development of efficient empirical and semi-analytical equations that can be used to replicate the centrifuge test displacements. The empirical method, based on the framework from Marshall et al. (2012), can be used to determine vertical movements; the new equations give improved performance at low cover-to-diameter ratios and extend the previous work by also considering the effect of soil relative density. Empirical expressions were also provided that give the relationship between surface and subsurface soil volume losses for varying soil relative density. Finally, a framework for the prediction of settlement trough shape based on the modified Gaussian

Table 2
Coefficients of the corrective terms ξ_z and ξ_x.

| C/D | 1.3 | 1.3 | 1.3 | 2 | 2 | 2 | 2.5 | 2.4 | 4.5 | 4.5 | 4.4 | 6.3 | 6.3 | 6.3 |
L_d	0.3	0.5	0.9	0.3	0.5	0.9	0.3	0.9	0.3	0.5	0.9	0.3	0.5	0.9
$m_{a,z}$	$-9.8E-02$	$-1.3E-01$	$-8.5E-02$	$-5.7E-02$	$-1.8E-01$	$-2.2E-01$	$-1.3E-01$	$-1.6E-01$	$-2.5E-02$	$-1.0E-01$	$-1.5E-01$	$-1.2E-01$	$-1.3E-01$	$-1.3E-02$
$q_{a,z}$	$1.5E+00$	$1.3E+00$	$1.0E+00$	$1.9E+00$	$1.7E+00$	$1.4E+00$	$2.2E+00$	$1.5E+00$	$2.2E+00$	$1.6E+00$	$1.9E+00$	$2.6E+00$	$2.8E+00$	$1.2E+00$
$m_{b,z}$	$1.2E-01$	$1.5E-01$	$3.0E-01$	$2.2E-01$	$3.0E-01$	$2.8E-01$	$1.0E-01$	$2.0E-01$	$3.4E-01$	$1.4E-01$	$3.0E-02$	$3.2E-01$	$7.6E-01$	$1.6E-01$
$q_{b,z}$	$0.0E+00$	$0.0E+00$	$0.0E+00$	$0.0E+00$	$0.0E+00$	$0.0E+00$	$0.0E+00$	$0.0E+00$	$0.0E+00$	$0.0E+00$	$0.0E+00$	$0.0E+00$	$0.0E+00$	$0.0E+00$
$m_{1,z}$	$3.6E-01$	$3.9E-01$	$5.9E-01$	$4.0E-01$	$5.4E-01$	$1.0E+00$	$1.2E-01$	$1.1E-01$	$2.2E-14$	$2.7E-01$	$2.3E-14$	$2.2E-14$	$2.2E-14$	$4.2E-02$
$q_{1,z}$	$1.0E+00$	$1.1E+00$	$8.7E-01$	$1.2E+00$	$3.0E-01$	$1.1E-12$	$1.1E+00$	$1.4E+00$	$1.5E+00$	$1.6E+00$	$1.1E+00$	$1.7E+00$	$1.2E+00$	$9.7E-01$
$m_{2,z}$	$2.2E-01$	$1.3E-01$	$2.5E-01$	$1.6E-01$	$1.8E-01$	$3.7E-01$	$1.5E-01$	$1.4E-01$	$6.7E-02$	$5.4E-02$	$1.4E-01$	$-1.7E-02$	$1.2E-01$	$1.2E-01$
$q_{2,z}$	$-1.7E-01$	$1.1E-01$	$-2.5E-01$	$-5.3E-01$	$1.6E-01$	$-7.5E-01$	$-7.3E-01$	$4.9E-02$	$-7.5E-01$	$-7.5E-01$	$-4.0E-01$	$-7.5E-01$	$-7.5E-01$	$1.2E-01$
$m_{3,z}$	$1.3E+00$	$5.1E-01$	$1.6E+00$	$4.1E-01$	$6.7E-01$	$1.6E+00$	$2.6E-01$	$1.2E+00$	$1.6E+01$	$1.7E-01$	$1.7E+01$	$3.8E+01$	$6.4E+01$	$6.8E+01$
$q_{3,z}$	0	0	0	0	0	0	0	0	0	0	0	0	0	0
$m_{4,z}$	0	0	0	0	0	0	0	0	0	0	0	0	0	0
$q_{4,z}$	$7.3E-01$	$7.3E-01$	$7.3E-01$	$8.0E-01$	$8.0E-01$	$8.0E-01$	$8.3E-01$	$8.3E-01$	$9.0E-01$	$9.0E-01$	$9.0E-01$	$9.3E-01$	$9.3E-01$	$9.3E-01$
$m_{5,z}$	$3.1E+00$	$4.1E+00$	$5.5E+00$	$2.6E+00$	$5.5E+00$	$7.7E+00$	$3.5E+00$	$1.2E+01$	$1.0E+00$	$1.0E+00$	$1.0E+00$	$1.0E+00$	$4.2E+00$	$1.0E+00$
$q_{5,z}$	0	0	0	0	0	0	0	0	0	0	0	0	0	0
$m_{6,z}$	0	0	0	0	0	0	0	0	0	0	0	0	0	0
$q_{6,z}$	$1.0E-01$	$1.0E-01$	$1.0E-01$	$1.0E-01$	$1.0E-01$	$1.0E-01$	$1.0E-01$	$1.0E-01$	$1.0E-01$	$1.0E-01$	$1.0E-01$	$1.0E-01$	$1.0E-01$	$1.0E-01$
$m_{b,x}$	$1.2E-01$	$1.5E-01$	$3.0E-01$	$2.2E-01$	$3.0E-01$	$2.8E-01$	$1.0E-01$	$2.0E-01$	$1.6E-01$	$2.4E-14$	$3.0E-02$	$7.3E-02$	$3.1E-01$	$1.6E-02$
$q_{b,x}$	0	0	0	0	0	0	0	0	0	0	0	0	0	0
$m_{1,x}$	$4.3E-01$	$7.0E-01$	$1.8E-06$	$4.3E-02$	$3.5E-01$	$2.4E-01$	$7.2E-07$	$3.0E-14$	$2.8E-04$	$1.1E+01$	$4.8E-01$	$2.3E-05$	$4.6E-01$	$2.0E+00$
$q_{1,x}$	$2.5E+00$	$1.5E+00$	$2.9E+00$	$6.4E+00$	$2.8E+00$	$1.7E+00$	$3.9E+00$	$7.1E+00$	$2.6E+01$	$2.8E-11$	$5.0E+00$	$1.3E+01$	$4.2E+00$	$8.3E-06$
$m_{2,x}$	$9.5E-02$	$7.6E-02$	$7.2E-02$	$-8.2E-02$	$3.9E-02$	$4.0E-01$	$-8.9E-02$	$-2.8E-02$	$-7.9E-01$	$-1.8E-01$	$-3.6E-01$	$-2.7E-01$	$3.5E-02$	$3.0E-01$
$q_{2,x}$	$2.1E-01$	$1.3E-01$	$3.6E-01$	$8.0E-01$	$5.1E-01$	$-3.4E-01$	$6.4E-01$	$1.4E+00$	$4.4E+00$	$2.1E+00$	$2.4E+00$	$2.3E+00$	$1.7E+00$	$-2.5E-01$

$m_{a,z} = m_{a,x}, q_{a,z} = q_{a,x}; m_{3,z} = m_{3,x}, q_{3,z} = q_{3,x}; m_{4,z} = m_{4,x}, q_{4,z} = q_{4,x}; m_{5,z} = m_{5,x}, q_{5,z} = q_{5,x}; m_{6,z} = m_{6,x}, q_{6,z} = q_{6,x}.$
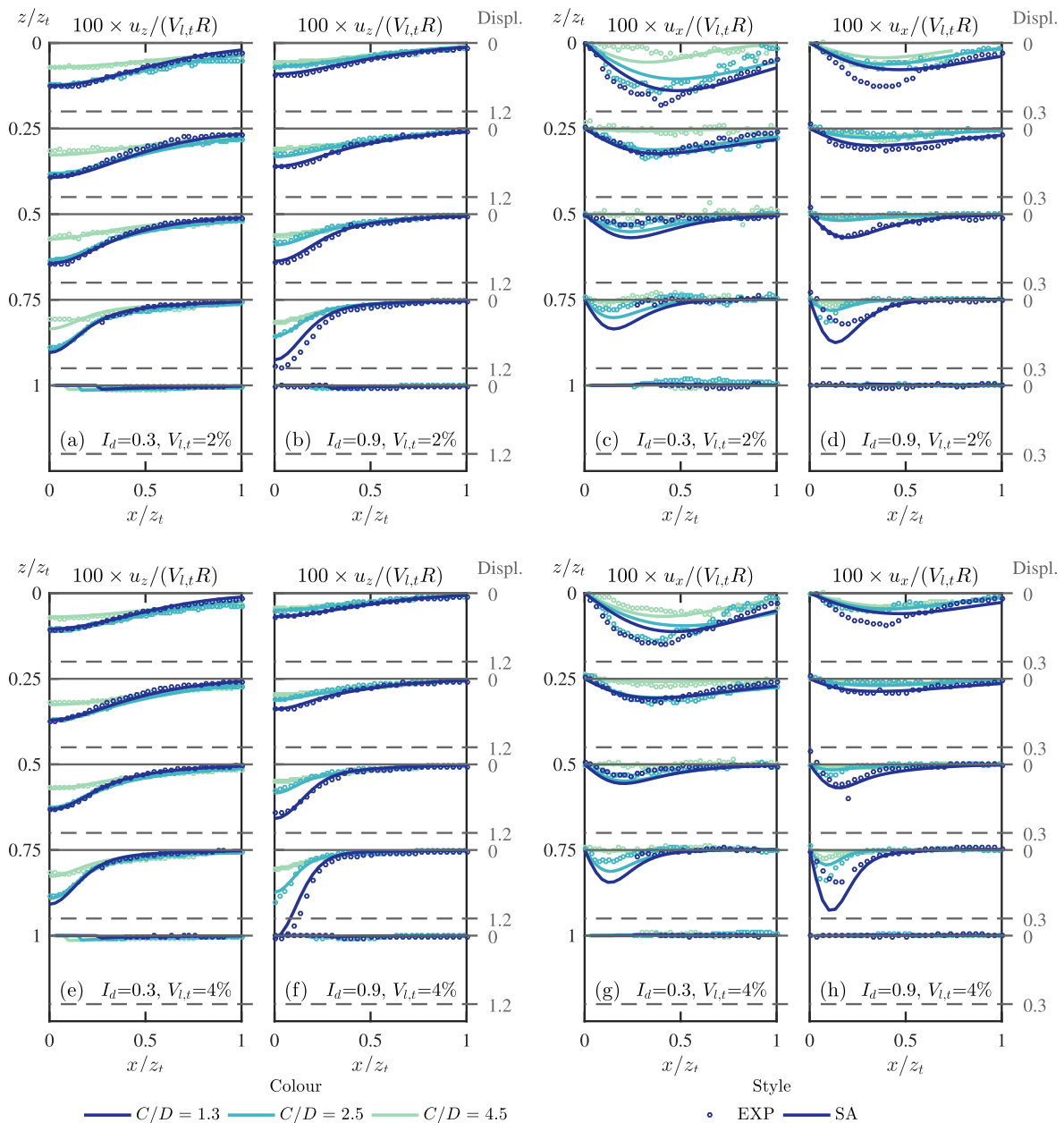
Fig. 12. Horizontal and vertical displacements in loose (a,c,e,f) and dense (b,d,f,h) sands for $V_{l,t} = 2\%$ and 4%: comparison between experimental and semi-analytical profiles.

curve was provided (Appendix A), which provides a straightforward approach that can be readily applied by researchers and engineers.

When subsurface and horizontal ground movements are used for tunnel-structure interaction analyses, it is necessary to assume a consistent soil deformation pattern. A computationally efficient semi-analytical solution involving the modification of an existing elastic analytical solution for incompressible soil was presented for the replication of vertical and horizontal ground movements obtained from centrifuge testing. This solution is able to account for the complex effects of tunnel volume loss, cover-to-diameter ratio, and soil relative density observed in sands, something that has not previously been achieved.

With appropriate judgement, the proposed empirical and semi-analytical equations can be used to define the input for tunnel-soil-structure interaction analyses. These inputs are most directly applicable to soil-structure interaction tests done with comparable centrifuge test methods. Once validated with the centrifuge test outcomes, the soil-structure interaction analyses could be more widely applied to other scenarios and used within design and risk-evaluation exercises.
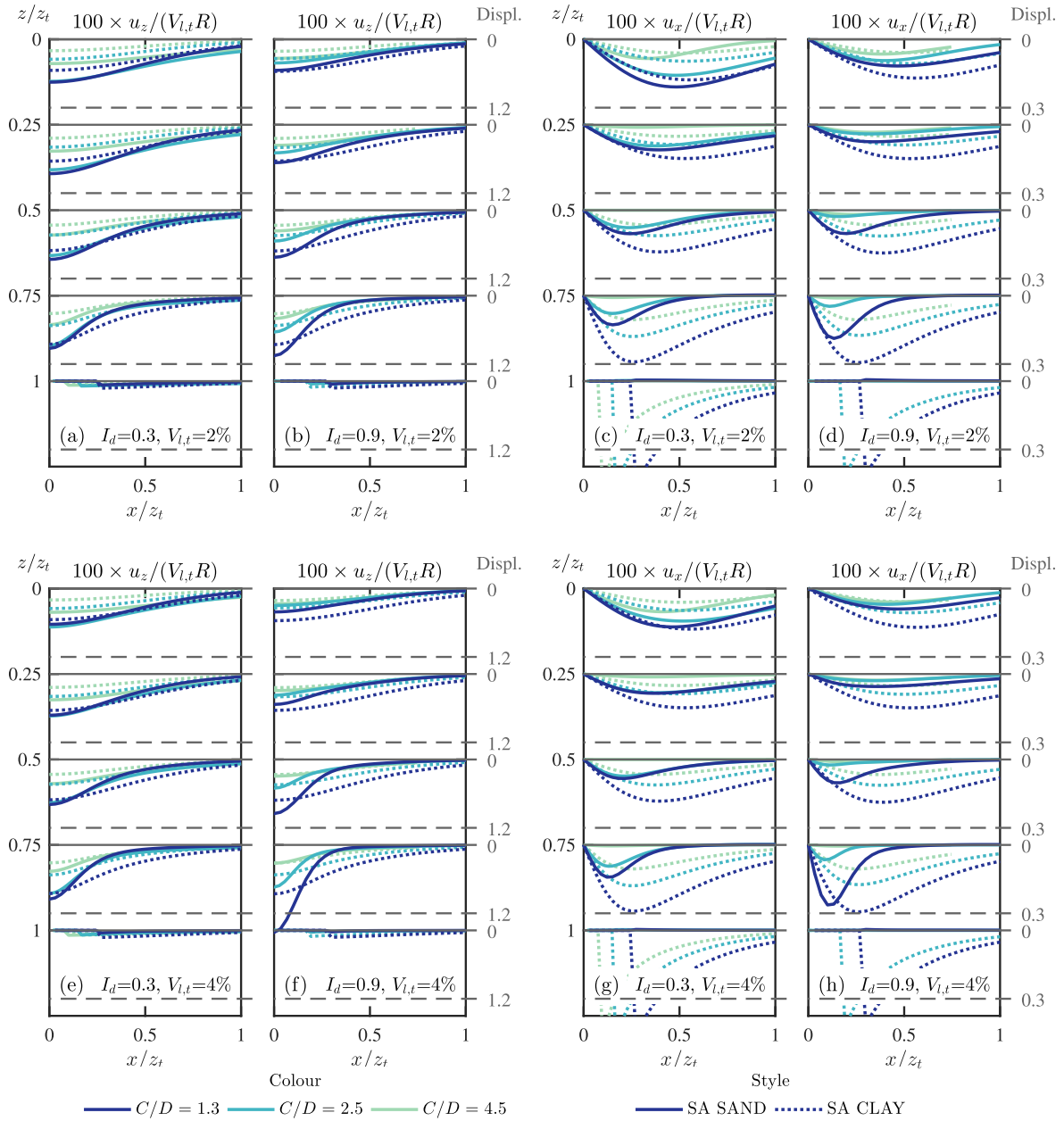
Acknowledgements

Fig. 13. Horizontal and vertical displacements for $V_{l,t} = 2\%$ and 4%: comparison between profiles in clays against those in loose (a,c,e,f) and dense (b,d,f,h) sands.

Appendix A

A.1. Equations of the modified Gaussian curve

The modified Gaussian curve is defined in Eq. (4). It has three degrees of freedom (a and i defining the shape and $u_{z,max}$ defining the magnitude), where the conditions $a > 0$, $n > 0$ and $i \neq 0$ guarantee the physical sense of the equation as a settlement trough.

In the empirical approaches, the modified Gaussian curve shape was defined through x^* and x^{**}. From the definition of x^* and x^{**}, we may obtain

$$\left(\frac{x^*}{i}\right)^2 = \frac{\ln[n\sqrt{e} - (n-1)]}{a} \tag{20}$$

$$\left(\frac{x^{**}}{i}\right)^2 = \frac{\ln[2n\sqrt{e} - (n-1)]}{a} \tag{21}$$

Combining Eqs. (5), (20) and (21) results in

$$\left(\frac{K^*}{K^{**}}\right)^2 = \frac{\ln[n\sqrt{e} - (n-1)]}{\ln[2n\sqrt{e} - (n-1)]} \tag{22}$$

The lower limit of K^*/K^{**} was obtained from

$$\lim_{n \to 0} \left(\frac{K^*}{K^{**}} \right)^2 = \lim_{n \to 0} \frac{\ln[n\sqrt{e} - (n-1)]}{\ln[2n\sqrt{e} - (n-1)]} = \frac{\sqrt{e} - 1}{2\sqrt{e} - 1} \tag{23}$$

Therefore, to guarantee $a > 0$ and $n > 0$

$$\left(\frac{K^*}{K^{**}} \right) > \sqrt{\frac{\sqrt{e} - 1}{2\sqrt{e} - 1}} \approx 0.532 \tag{24}$$

From Eq. (20), the inflection point offset is given by

$$i = \pm \sqrt{\frac{ax^{*2}}{\ln[n\sqrt{e} - (n-1)]}} \tag{25}$$

A.2. Degrees of freedom from the empirical method

The following approximate set of equations can be used to estimate the degrees of freedom of the modified Gaussian curve (a, i, $u_{z,max}$) from the parameters of the empirical method (K^*, K^{**}, $V_{l,s}$).

$$K^{**} \leqslant 1.85K^*$$
$$a \approx 10^{-7} \exp\left[-17.5\left(\frac{K^*}{K^{**}} \right)^2 + 35.5\left(\frac{K^*}{K^{**}} \right) \right] - 0.11$$
$$i = \sqrt{\frac{a}{\ln[n\sqrt{e} - (n-1)]}} \times K^*(z_t - z)$$
$$u_{z,max} \approx \frac{\sqrt{2\pi}}{\exp[1.7 + 0.52a - 1.47\sqrt{a}]} \times \frac{V_{l,s}\pi R^2}{100i\sqrt{2\pi}} \tag{26}$$

This approximation is valid for $K^*/K^{**} = 0.54 - 0.75$, which covers the typical range of a.

Appendix B

See Table 2.

Appendix C. Supplementary material

Supplementary data associated with this article can be found, in the online version, at https://doi.org/10.1016/j.tust.2019.02.016.

References

Basile, F., 2014. Effects of tunnelling on pile foundations. Soils Found. 54 (3), 280–295.

Basmaji, B., Deck, O., Al Heib, M., 2017. Analytical model to predict building deflections induced by ground movements. Eur. J. Environ. Civ. Eng. 1–23 feb.

Bilotta, E., Russo, G., 2012. Ground movements induced by tunnel boring in Naples. In: Viggiani, G. (Ed.), Proc., 7th Int. Symp. Geotech. Asp. Undergr. Constr. Soft Gr. CRC Press, London, Rome, Italy, pp. 979–986.

Celestino, T.B., Gomes, R.A.M.P., Bortolucci, A.A., 2000. Errors in ground distortions due to settlement trough adjustment. Tunn. Undergr. Sp. Technol. 15 (1), 97–100.

Dias, D., Kastner, R., 2013. Movements caused by the excavation of tunnels using face pressurized shields - Analysis of monitoring and numerical modeling results. Eng. Geol. 152 (1), 17–25 jan.

Dias, T.G.S., Bezuijen, A., 2017. Pile tunnel interaction: an analytical framework. In: Geotech. Asp. Undergr. Constr. Soft Gr. Proc. 9th Int. Symp. Geotech. Asp. Undergr. Constr. Soft Grounds. CRC Press, Sao Paulo, Brazil, pp. 105–110.

Dimmock, P.S., Mair, R.J., 2007. Estimating volume loss for open-face tunnels in London Clay. Proc. ICE -Geotechnical Eng. January (GE I) 13–22.

Fargnoli, V., Boldini, D., Amorosi, A., 2013. TBM tunnelling-induced settlements in coarse-grained soils: The case of the new Milan underground line 5. Tunn. Undergr. Sp. Technol. 38, 336–347.

Farrell, R., 2010. Tunnelling in sands and the response of buildings. Ph.D. Thesis, Cambridge Univ.

Farrell, R., Mair, R., Sciotti, A., Pigorini, A., 2014. Building response to tunnelling. Soils Found. 54 (3), 269–279.

Franza, A., 2016. Tunnelling and its effects on piles and piled structures. Ph.D. Thesis, Univ. Nottingham.

Franza, A., Marshall, A.M., 2015a. Analytical investigation of soil deformation patterns above tunnels in sandy soil. In: In: Smith, D., Eldred, P., Winter, M., Eldred, P., Toll, D., Winter, M. (Eds.), Proc. XVI ECSMGE Geotech. Eng. Infrastruct. Dev Vol. 2. ICE Publishing, Edinburgh, United Kingdom, pp. 467–472.

Franza, A., Marshall, A.M., 2015b. Semi-analytical prediction of ground movements due to shallow tunnels in sand. In: In: Smith, D., Eldred, P., Winter, M., Eldred, P., Toll, D., Winter, M. (Eds.), Proc. XVI ECSMGE Geotech. Eng. Infrastruct. Dev Vol. 2. ICE Publishing, Edinburgh, United Kingdom, pp. 461–466.

Franza, A., Marshall, A.M., 2018. Centrifuge modeling study of the response of piled structures to tunneling. J. Geotech. Geoenviron. Eng. 144 (2), 04017109 feb.

Franza, A., Marshall, A.M., Haji, T., Abdelatif, A.O., Carbonari, S., Morici, M., 2017. A simplified elastic analysis of tunnel-piled structure interaction. Tunn. Undergr. Sp. Technol. 61, 104–121.

Franza, A., Marshall, A.M., Zhou, B., 2019. Greenfield tunnelling in sands: the effects of soil density and relative depth. Géotechnique (in press). https://doi.org/10.1680/jgeot.17.P.091.

Franza, A., Zhou, B., Marshall, A.M., 2016. The effects of relative tunnel depth and volume loss on vertical settlements above tunnels in dense sands. In: Ni, J.C., Yang, J., Chen, S.-l., Qiu, T. (Eds.), Proc. 4th Geo-China Int. Conf. No. 260 GSP. American Society of Civil Engineers (ASCE), Shandong, China, pp. 125–132.

Fu, J., Yang, J., Klapperich, H., Wang, S., 2016. Analytical prediction of ground movements due to a nonuniform deforming tunnel. Int. J. Geomech. 16 (4), 04015089.

Giardina, G., DeJong, M.J., Mair, R.J., 2015. Interaction between surface structures and tunnelling in sand: Centrifuge and computational modelling. Tunn. Undergr. Sp. Technol. 50, 465–478.

González, C., Sagaseta, C., 2001. Patterns of soil deformations around tunnels. Application to the extension of Madrid Metro. Comput. Geotech. 28 (6?7), 445–468.

Grant, R.J., Taylor, R.N., 2000. Tunnelling-induced ground movements in clay. Proc. ICE - Geotech. Eng. 143 (1), 43–55.

Haji, T.K., Marshall, A.M., Franza, A., 2018a. Mixed empirical-numerical method for investigating tunnelling effects on structures. Tunn. Undergr. Sp. Technol. 73, 92–104.

Haji, T.K., Marshall, A.M., Tizani, W., 2018b. A cantilever approach to estimate bending stiffness of buildings affected by tunnelling. Tunn. Undergr. Sp. Technol. 71, 47–61.

Hsiung, B.C.B.B.-C., 2011. A case record of bored tunnels in sand based on the Kaohsiung mass rapid transit system project. J. Geoengin. 6 (3), 113–123.

Huang, M., Mu, L., 2012. Vertical response of pile raft foundations subjected to tunneling-induced ground movements in layered soil. Int. J. Numer. Anal. Methods Geomech. 36 (8), 977–1001.

Ieronymaki, E., Whittle, A.J., Einstein, H.H., 2018. Comparative study of the effects of three tunneling methods on ground movements in stiff clay. Tunn. Undergr. Sp. Technol. 74, 167–177 apr.

Ieronymaki, E.S., Whittle, A.J., Sureda, D.S., 2016. Interpretation of free-field ground movements caused by mechanized tunnel construction. J. Geotech. Geoenviron. Eng. 4016114.

Jones, B., 2010. Low-volume-loss tunnelling for London ring main extension. Proc. ICE -Geotech. Eng. 163 (3), 167–185.

Kitiyodom, P., Matsumoto, T., Kawaguchi, K., 2005. A simplified analysis method for piled raft foundations subjected to ground movements induced by tunnelling. Int. J. Numer. Anal. Methods Geomech. 29 (15), 1485–1507.

Klar, A., Elkayam, I., Marshall, A.M., 2015. Design oriented linear-equivalent approach for evaluating the effect of tunneling on pipelines. J. Geotech. Geoenviron. Eng. 142 (1), 04015062.

Klar, A., Marshall, A.M., 2008. Shell versus beam representation of pipes in the evaluation

of tunneling effects on pipelines. Tunn. Undergr. Sp. Technol. 23 (4), 431–437.

Klar, A., Marshall, A.M., 2015. Linear elastic tunnel pipeline interaction: the existence and consequence of volume loss equality. Géotechnique l (9), 1–5.

Klar, A., Vorster, T.E., Soga, K., Mair, R.J., 2007. Elastoplastic solution for soil-pipe-tunnel interaction. J. Geotech. Geoenviron. Eng. 133 (7), 782–792.

Lee, C.-J.J., Chiang, K.-H.H., 2007. Responses of single piles to tunneling-induced soil movements in sandy ground. Can. Geotech. J. 44 (10), 1224–1241 oct.

Lee, K.M., Rowe, R.K., Lo, K.Y., 1992. Subsidence owing to tunnelling. I. Estimating the gap parameter. Can. Geotech. J. 29 (6), 929–940.

Li, P., Du, S.-J., Shen, S.-L., Wang, Y.-H., Zhao, H.-H., 2015. Timoshenko beam solution for the response of existing tunnels because of tunneling underneath. Int. J. Numer. Anal. Methods Geomech.

Loganathan, N., Poulos, H.G., 1998. Analytical prediction for tunneling-induced ground movements in clays. J. Geotech. Geoenviron. Eng. 124 (9), 846–856.

Mair, R.J., 1979. Centrifugal modelling of tunnel construction in soft clay. PhD Thesis Cambridge Univ.

Mair, R.J., Taylor, R.N., 1993. Prediction of clay behaviour around tunnels using plasticity solutions. In: Telford, T. (Ed.), Predict. Soil Mech. Proc. Wroth Meml. Symp. Held St. Catherine's Coll. Oxford, pp. 449–463.

Mair, R.J., Taylor, R.N., 1997. Theme lecture: Bored tunnelling in the urban environment. In: 14th Int. Conf. soil Mech. Found. Eng. Balkema, Hamburg, pp. 2353–2385.

Mair, R.J., Taylor, R.N., Bracegirdle, A., 1993. Subsurface settlement profiles above tunnels in clay. Géotechnique 43 (2), 315–320.

Mair, R.J., Taylor, R.N., Burland, J.B., 1996. Prediction of ground movements and assessment of risk of building damage due to bored tunnelling. In: Mair, R.J., Taylor, R. N. (Eds.), Proc. Int. Symp. Geotech. Asp. Undergr. Constr. Soft Gr. Balkema, Rotterdam, London, United Kingdom, pp. 713–718.

Marshall, A.M., 2009. Tunnelling in sand and its effect on pipelines and piles. Ph.D. Thesis, Cambridge Univ.

Marshall, A.M., Farrell, R., Klar, A., Mair, R., 2012. Tunnels in sands: the effect of size, depth and volume loss on greenfield displacements. Géotechnique 62 (5), 385–399.

Mo, P.-Q., Yu, H.-S., 2017. Undrained cavity-contraction analysis for prediction of soil behavior around tunnels. Int. J. Geomech. 17 (5), 04016121.

Mu, L., Huang, M., Finno, R.J., 2012. Tunnelling effects on lateral behavior of pile rafts in layered soil. Tunn. Undergr. Sp. Technol. 28, 192–201 mar.

Peck, R.B., 1969. Deep excavations and tunnelling in soft ground. In: Proc. 7th Int. Conf. Soil Mech. Found. Eng. Mexico City, Mexico, pp. 225–290.

Pender, M.J., 1980. Elastic solutions for a deep circular tunnel. Géotechnique 30 (2), 216–222.

Pinto, F., Whittle, A.J., 2006. Discussion of Elastic solution for tunneling-induced ground movements in clays by K.H. Park. Int. J. Geomech. 6 (1), 72–73.

Pinto, F., Zymnis, D.M., Whittle, A.J., 2014. Ground movements due to shallow tunnels in soft ground. II: Analytical interpretation and prediction. J. Geotech. Geoenviron. Eng. 140 (4), 1–11 apr.

Potts, D.M., 1976. Behaviour of lined and unlined tunnels in sand. Ph.D. thesis, Cambridge Univ.

Ritter, S., Giardina, G., DeJong, M.J., Mair, R.J., 2017. Influence of building characteristics on tunnelling-induced ground movements. Géotechnique 67 (10), 926–937.

Rowe, R., Kack, G., 1983. A theoretical examination of the settlements induced by

tunnelling: four case histories. Can. Geotech. J. 20 (2), 299–314.

Sagaseta, C., 1987. Analysis of undrained soil deformation due to ground loss. Géotechnique 37 (3), 301–320 jan.

Sagaseta, C., Sanchez-Alciturri, J.M., Gonzalez, C., Lopez, A., Gomez, J., Pina, R., 1999. Soil deformations due to the excavation of two parallel caverns. In: Proc. 12th Eur. Conf. Soil Mech. Geotech. Eng., vol. 3. A.A. Balkema, pp. 2125–2131.

Son, M., 2015. Response analysis of nearby structures to tunneling-induced ground movements in sandy soils. Tunn. Undergr. Sp. Technol. 48, 156–169.

Son, M., 2016. Response analysis of nearby structures to tunneling-induced ground movements in clay soils. Tunn. Undergr. Sp. Technol. 56, 90–104.

Strack, O.b., Verruijt, A., 2002. A complex variable solution for a deforming buoyant tunnel in a heavy elastic half-plane. Int. J. Numer. Anal. Methods Geomech. 26 (12), 1235–1252.

Sugiyama, T., Hagiwara, T., Nomoto, T., Nomoto, M., Ano, Y., Mair, R., Bolton, M., Soga, K., 1999. Observations of ground movements during tunnel construction by slurry shield method at the Docklands Light Railway Lewisham Extension-East London. Soils Found. 39 (3), 99–112.

van Jaarsveld, E.P., Plekkenpol, J.W., van de Graaf, C.A.M., 1999. Ground deformations due to the boring of the Second Heinenoord Tunnel. In: Geotech. Eng. Transp. infrastructure. Proc. 12th Eur. Conf. soil Mech. Geotech. Eng., vol. 1. A.A. Balkema, Amsterdam, pp. 153–159.

Verruijt, A., 1997. A complex variable solution for a deforming circular tunnel in an elastic half-plane. Int. J. Numer. Anal. Methods Geomech. 21 (2), 77–89.

Verruijt, A., Booker, J., 1996. Surface settlements due to deformation of a tunnel in an elastic half plane. Géotechnique 46 (4), 753–756.

Verruijt, A., Strack, O., 2008. Buoyancy of tunnels in soft soils. Géotechnique 58 (6), 513–515.

Vorster, T.E.B., Klar, A., Soga, K., Mair, R.J., 2005. Estimating the effects of tunneling on existing pipelines. J. Geotech. Geoenvirom. Eng. 131 (11), 1399–1410 nov.

Vu, M.N., Broere, W., Bosch, J., 2016. Volume loss in shallow tunnelling. Tunn. Undergr. Sp. Technol. 59, 77–90.

White, D., Take, W., Bolton, M., 2003. Soil deformation measurement using particle image velocimetry (PIV) and photogrammetry. Géotechnique 53 (7), 619–631 jan.

Yu, J., Zhang, C., Huang, M., 2013. Soil-pipe interaction due to tunnelling: assessment of Winkler modulus for underground pipelines. Comput. Geotech. 50, 17–28.

Zhang, R.J., Zheng, J.J., Yu, S., 2013. Responses of piles subjected to excavation-induced vertical soil movement considering unloading effect and interfacial slip characteristics. Tunn. Undergr. Sp. Technol. 36, 66–79.

Zhang, R.J., Zheng, J.J., Zhang, L.M., Pu, H.F., 2011. An analysis method for the influence of tunneling on adjacent loaded pile groups with rigid elevated caps. Int. J. Numer. Anal. Methods Geomech. 35 (18), 1949–1971.

Zhang, Z., Huang, M., Xi, X., Yang, X., 2018. Complex variable solutions for soil and liner deformation due to tunneling in clays. Int. J. Geomech. 18 (7), 04018074.

Zhou, B., 2014. Tunnelling-induced ground displacements in sand. Ph.D. Thesis, Univ. Nottingham.

Zhou, B., Marshall, A.M., Yu, H.-S., 2014. Effect of relative density on settlements above tunnels in sands. In: 2014 GeoShanghai Int. Congr. Tunneling Undergr. Constr., vol. 242 GSP. American Society of Civil Engineers, Shanghai, China, pp. 96–105.